IEEE Access
Multidisciplinary ⋮ Rapid Review ⋮ Open Access Journal

Received 15 March 2024, accepted 21 March 2024, date of publication 27 March 2024, date of current version 16 April 2024.

Digital Object Identifier 10.1109/ACCESS.2024.3381968

RESEARCH ARTICLE

Interference Management for VLC Indoor Systems Based on Overlapping Field-of-View Angle Diversity Receivers

AHMED GAAFAR AHMED AL-SAKKAF AND MÁXIMO MORALES-CÉSPEDES, (Member, IEEE)
Department of Signal Theory and Communications, Universidad Carlos III de Madrid, 28911 Leganés, Spain

Corresponding author: Ahmed Gaafar Ahmed Al-Sakkaf (aasakkaf@tsc.uc3m.es)

This work was supported in part by European Union (EU) Horizon 2020 Research and Innovation Program through the Marie Skłodowska-Curie European Training Networks (ETN) TeamUp5G under Grant 813391, and in part by Ministerio de Ciencia, Innovación y Universidades (MICIU)/Agencia estatal de investigación (AEI)/10.13039/501100011033 and Unión Europea NextGenerationEU/Plan de Recuperacion, Transformación y Resiliencia (PRTR) under Project TED2021-129869B-I00. The work of Máximo Morales-Céspedes was supported in part by the Juan de la Cierva Incorporación Program under Grant IJC2019-040317-I MICIU/AEI/10.13039/501100011033, and in part by the Ramón y Cajal Program under Grant RYC2022-036053-I (MICIU/AEI/10.13039/501100011033 and FSE+).

ABSTRACT The integration of visible light communications (VLC) in future generation of wireless communications leads to consider the deployment of multiple access points (APs) transmitting in the optical domain. Since each optical AP generates a small and confined coverage footprint, scenarios comprising multiple optical APs are subject to intercell interference. In this context, angle diversity receivers (ADRs) composed of multiple photodiodes pointing to distinct orientations each, have been proposed for mitigating the interference and blocking effects. The design of ADRs typically assumes that the field-of-view (FoV) generated by each photodiode does not overlap with the FoV of all other photodiodes. In this work, we propose the derivation of the theoretical expressions of the probability distribution function (PDF) and the cumulative distribution function (CDF) of the signal-to-interference plus noise ratio (SINR) in multicell scenarios for ADRs in which the FoV generated by each photodiode may overlap with the FoV of the other photodiodes. Several geometrical conditions are proposed in order to derive the statistical characterization of photodiode combining schemes such as select best combining (SBC), equal gain combining (EGC) and maximum ratio combining (MRC). It is shown that the derived closed-form expressions obtain a similar performance as the results obtained through Monte Carlo simulations. Moreover, the SINR enhancement due to the use of the proposed ADR in comparison with single photodiode receivers is highlighted.

INDEX TERMS Interference management, visible light communications, signal-to-interference plus noise ratio (SINR), angle diversity receiver (ADR).

I. INTRODUCTION

Visible light communication (VLC) is a promising technology for the next generation of wireless communications, including the evolution to 6G [1]. Compared to traditional communication technologies, VLC offers several advantages, such as a wide and unregulated bandwidth, low-latency or improved security due to the small and confined coverage footprint generated by each optical access point (AP). Moreover, VLC is useful for unloading the overwhelmed radio-frequency (RF) spectrum by moving part of the indoor data traffic to the optical domain. During the last decade, several potential applications such as positioning, sensing or vehicular and underwater communications have been proposed based on VLC [2], [3], [4].

Integrating optical APs into cellular networks lead to several advantages such as increasing the network capacity and coverage while providing satisfactory illumination. The

The associate editor coordinating the review of this manuscript and approving it for publication was Barbara Masini.

optical APs are indeed considered as active element of the heterogeneous cellular networks, usually referred to as *attocells*. However, the deployment of multiple optical APs may lead to intercell interference at cell edge of the coverage footprint generated by each optical AP. It is worth noticing that frequency reuse (FR), widely applied in cellular networks, may not be applied to VLC because of the limited coverage footprint of each optical AP. That is, FR would perform frequency switching every few meters, which results challenging to implement in practice [5]. On the other hand, advanced interference management techniques such as transmit precoding schemes (TPC), e.g., linear zero forcing (ZF) [6], which require indeed additional resources for RF systems for estimating the channel state information (CSI), result even more complex in VLC systems. The small-scale effects that generate a rich scattering environment in RF systems do not affect to VLC, which may generate highly correlated channel responses [7], [8]. Besides, VLC is inherently based on frequency division duplex (FDD). Therefore, achieving CSI requires the transmission of pilots and feed the estimated channel back to the transmitters via uplink.

Angle diversity receivers (ADRs) have been proposed for uncorrelating the channel responses in VLC enabling to achieve high data rate, mitigating the blocking effects or enhancing the coverage footprint generated by the optical APs [9], [10]. Basically, an ADR is composed of multiple photodiodes following an angular diversity arrangement as it is shown in Fig. 1. In [11], two arrangements named pyramidal and hemispherical ADRs are proposed. The design of the ADRs can be improved considering the use of lenses such as compound parabolic concentrators (CPCs) as proposed in [12]. Then, ADRs have been proposed for managing the intercell interference at the receiver side in several VLC applications such as vehicular [13] or underground mining [14], [15]. Key findings from experimental investigations of vehicular VLC using ADRs are presented in [13] and [16]. The hemidodecahedron structure was proposed in [14] to mitigate intercell interference and enhancing the achievable rate. Subsequently, the hemidodecahedron structure was introduced in underground mining VLC systems to estimate the optimal angle of incidence and orientation of the receiver [17].

At this point, it is possible to differentiate between overlapping and non-overlapping field of view (FoV) ADRs as it is shown in Fig. 1. In this sense, non-overlapping ADRs have been a common approach for theoretical analysis of the SINR since it allows us to discriminate the signal received in a single photodiode from the whole set of photodiodes that compose the receiver. Based on this non-overlapping approach, the statistical distribution of the SINR assuming a simple receiver architecture in which a single photodiode is pointing perpendicularly to the ceiling is derived in [18]. In [19], the probability density function (PDF) and the cumulative distribution function (CDF)

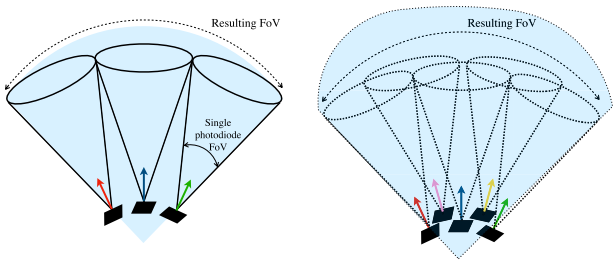

(a) ADR for non-overlapping FoVs. (b) ADR overlapping FoVs.

FIGURE 1. ADR architectures for non-overlapping and overlapping FoVs.

achieved by ADRs under photodiode combining schemes are derived. However, this work assumes a very narrow FoV for each photodiode that compose the ADR so that a unique photodiode receives a line-of-sight (LoS) contribution while managing the interference in the remaining photodiodes as a non-LoS (NLoS) contribution. This approach leads to a straightforward derivation of the PDF and CDF of the SINR by simply applying closed-form expressions of the cosine of the irradiance and incidence angles and the change of variable method afterwards.

However, non-overlapping ADRs may not result suitable from a practical perspective due to both the dimensional constraints of the VLC devices and the application of multiple-input multiple-output (MIMO) signal processing. In [20], the orientation of hand-held devices is statistically analyzed for ensuring a LoS contribution. Based on this work, an ADR providing signal detection in each of the six faces of the device is required to satisfy this condition. However, solving this issue following a non-overlapping approach may lead to an impractical solution due to the dimensional constraints of common receivers such as hand-held devices as depicted in Fig. 2. For instance, to achieve an optical gain of 33 for a FoV equal to 10° the length and collection area of the CPC are equal to 28.7 mm and 0.58 cm^2, respectively. Furthermore, receiving a LoS and uncorrelated contribution at multiple photodiodes, i.e., following an overlapping FoV ADR approach, results useful to apply MIMO signal processing processing [11], [21]. In such a way, the concept of constrained-FoV-ADR, in which the FoV angle is optimized so that the ADR generates a maximum of N_r LoS signal from N_t LEDs forming a $N_r \times N_t$ MIMO system, is proposed in [22].

In this work, we propose an alternative analysis of the ADRs in which the FoV of multiple photodiodes may overlap as illustrated in Fig. 1(b). Specifically, the statistical characterization of the SINR in the coverage footprint of each optical AP is derived and analyzed through Monte Carlo simulations. That is, this work faces the derivation of the PDF and CDF of the SINR in VLC indoor systems considering the implementation of overlapping FoV ADRs in practical devices. In this sense, the combination schemes select best combining (SBC), equal gain combining (EGC),

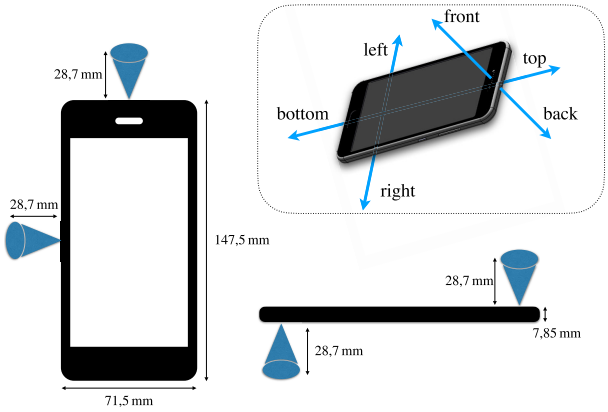

FIGURE 2. Deployment of an ADR in a hand-held device. The use of very narrow FoV photodiodes, e.g., 10° based on CPCs, may lead to an impractical implementation.

and maximum ratio combining (MRC) for the multiple photodiodes that compose the ADR are considered. The main contributions of this work can be summarized as follows:

1) ADRs in which the FoVs of the photodiodes overlap among them are considered. The geometrical analysis carried out shows that this approach ensures a wide FoV while providing at least a very directive LoS contribution, in which the assumption $\cos(\psi) = 1 - \epsilon$, where ψ represents the angle of incidence of at least one photodiode of the ADR and ϵ is a very small positive value, can be assumed.
2) The PDF and CDF of the SINR in a multicell scenario for the proposed ADR architecture are derived. Notice that in contrast to previous works, it is necessary to consider that more than one LoS contribution is received in the areas of the coverage footprint subject to intercell interference. In this sense, several geometrical conditions are proposed for obtaining closed-form expressions of the statistical characterization.
3) Simulation results show that the approach based on dividing the coverage footprint into two scenarios; cell center and edge where the intercell interference is mainly given the NLoS and LoS components, respectively, results appropriate. Moreover, the theoretical closed-form expressions of the statistical distribution of the SINR matches with the analytical results. The derived statistical characterization allows us to analyze the role of the number of photodiodes in the proposed ADR and the impact of the radiation semi-angle in a multicell VLC scenario. Furthermore, a discussion about implementing a real-world testing and some experimental results are also shown with the aim of validating the considered approach.

The proposed approach and the derived equations result useful for the design of VLC networks since they provide a tool, the statistical distribution of the SINR for overlapping FoV ADRs, as a function of the geometry of the scenario and the characteristics of the receiver. That is, they allow us to determine the impact of the deployment of optical APs (height, coverage radius, radiation semi-angle, etc.) as well as the number of photodiodes that compose the ADR on the SINR distribution for different schemes such as SBC or MRC. For instance, internet of things (IoT) services typically demand uniform SINR distributions and devices with a low complexity, i.e., composed of a single transimpedance amplifier and low computational capacity, which would correspond to a SBC scheme. On the other hand, the MRC scheme applied to receivers equipped with multiple photodiodes and some computational complexity is preferable for services demanding high-data rates. Furthermore, exploiting the knowledge associated with the statistical characterization of the SINR is also useful for predicting the behaviour of the datasets feeding the artificial intelligence algorithms [23], which may lead to a reduction of the need for obtaining additional measurements devoted to generate new and more realistic datasets.

The remainder of this paper is organized as follows. In Section II, the system model is presented, modeling the ADR architecture and both the LoS and NLoS contributions of the optical channel. For illustrative purposes, the SINR distribution for the single photodiode architecture is briefly described in Section III. In Section IV, the combining schemes for multiple photodiodes receiver architectures are presented. The statistical characterization of the SINR for the proposed ADR architecture, in which the FoVs of the photodiodes overlap among them, is derived in Section V. Section VI presents some simulation and experimental results. Finally, Section VII provides concluding remarks.

II. SYSTEM MODEL

We consider a VLC network composed of L, $l = \{1, \ldots, L\}$, optical APs that provide illumination and data transmission to K, $k = \{1, \ldots, K\}$, users equipped with an ADR each. The ADR of each user is composed of N_{PD}, $i = \{1, \ldots, N_{\text{PD}}\}$, photodiodes. Each user receives data from a single optical AP, while managing the interference from all other transmitters as noise. The transmitted signal from optical AP l is denoted by x_l. Then, the signal received from optical AP l by the photodiode i of a generic user is given by

$$y_i = H_{l,i}\, x_l + \sum_{l'=1, l' \neq l}^{L} H_{l',i}\, x_{l'} + n_0, \tag{1}$$

where $H_{l,i}$ is the channel between optical AP l and photodiode i, and $H_{l',i}$ is channel between the interfering optical AP $l' \neq l$, which transmits the signal $x_{l'}$, and n_0 represents the real valued additive white Gaussian noise with zero mean and variance $\sigma_n^2 = \sigma_{\text{shot}}^2 + \sigma_{\text{thermal}}^2$ where σ_{shot}^2 is the shot noise variance and $\sigma_{\text{thermal}}^2$ is the thermal noise variance [24].

A. ARCHITECTURE OF THE ANGLE DIVERSITY RECEIVERS

For the sake of simplicity, we consider both the single photodiode (single-PD) and pyramidal ADR architectures.

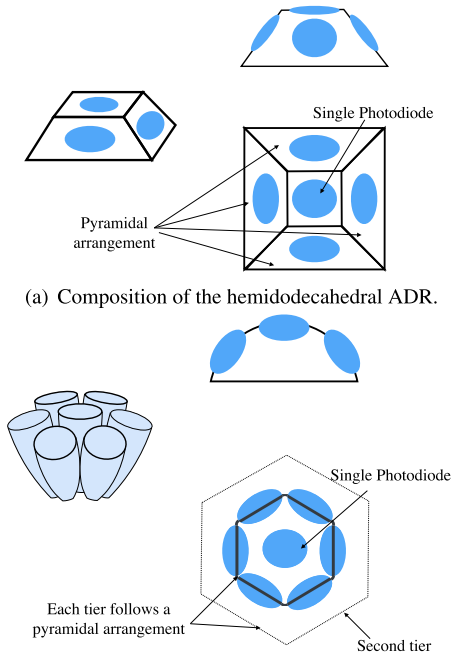

FIGURE 3. Composition of hemidodecahedral and *N*-tiers ADRs based on the pyramidal arrangement.

For single-PD, we assume that each user is equipped with a photodiode that points perpendicularly to the ceiling.

In this study, we focus on the pyramidal arrangement since it is one of the most common ADR structures. The pyramidal configuration is assumed because of the following two reasons; *i*) for the sake of clarity and replication of the obtained results and *ii*) it is a basic configuration that allows us to extend the derived statistical characterization to other more complex configurations. In this sense, notice that other photodiode arrangements such as hemidodecahedral [14], [15] or N-tiers ADRs [12] can be composed based on the pyramidal configuration as can be seen in Fig 3.

The pyramidal arrangement is composed of N_{PD} photodiodes allocated in each of the faces of a pyramid as can be seen in Fig. 4. Thus, the orientation vector of photodiode i of user k in can be written as

$$\hat{\mathbf{n}}_k(i) = [\sin(\theta_k)\cos(\alpha_k), \sin(\theta_k)\sin(\alpha_k), \cos(\theta_k)], \quad (2)$$

where the elevation and azimuthal angles are denoted by θ_k and α_k, respectively. Notice that the orientation vector of the single-PD architecture is simply given by $\hat{\mathbf{n}}_k = [0, 0, 1]$. Moreover, it is assumed that the optical APs are pointing to perpendicularly to the floor, i.e., the orientation vector of each optical AP is given by $\hat{\mathbf{n}}_l = [0, 0, -1]$. Then, the irradiance and incidence angles of each photodiode can be determined by

$$\varphi_{lk} = \arccos\left(\frac{\hat{\mathbf{n}}_l \cdot \mathbf{v}_{lk}}{\| \hat{\mathbf{n}}_l \| \| \mathbf{v}_{lk} \|}\right), \quad (3)$$

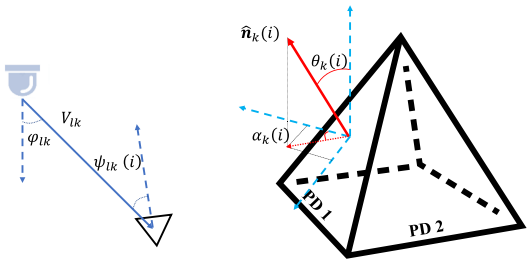

FIGURE 4. Pyramid ADR with four faces, the figure shows the both elevation and azimuthal θ_k and α_k respectively. Also it shows the angles irradiance and incident φ_{lk} and $\psi_{lk}(i)$ respectively.

and

$$\psi_{lk}(i) = \arccos\left(\frac{\mathbf{v}_{lk} \cdot \hat{\mathbf{n}}_k(i)}{\| \mathbf{v}_{lk} \| \| \hat{\mathbf{n}}_k(i) \|}\right), \quad (4)$$

where φ_{lk} and $\psi_{lk}(i)$ are the angles of irradiance[1] and incidence between the optical AP l and user k, respectively. The vector between the AP l and the user k is denoted by $\mathbf{v}_{lk}$, whereas $\hat{\mathbf{n}}_l$ is the pointing vector of the optical AP l as it is shown in Fig. 4. For the pyramidal architecture, all the photodiodes are subject to the same elevation angle θ_k while the azimuthal angle is uniformly distributed so that $\alpha_k(i) = \frac{2(i-1)\pi}{N_{\text{PD}}-1}$, $i = \{1, \ldots, N_{\text{PD}}\}$.

The described ADR approach can be easily implemented in practical devices. It is worth noticing that the pyramidal, or any other photodiode arrangement, does not involve to construct a pyramid, it refers exclusively to the orientation of the photodiodes along the receiver. Focusing on hand-held devices already manufactured, the integration of the photodiodes following an angular diversity arrangement can be implemented in bumpers or cellphone cases. On the other hand, the integration of ADRs can be carried out along the six faces of the new hand-held devices. Focusing on industrial applications, the ADR structures can be easily implemented in helmets as proposed in [22] using available tools, such as 3D printers. Furthermore, the integration of ADRs in vehicles can be carried out taking advantage of the structure of the vehicles, integrating the photodiodes and lenses within elements such as the head or back lights lamps or behind the windshield [3]. At this point, it is worth remarking that the proposed overlapping ADR approach relaxes the dimensional requirements in comparison with non-overlapping ADRs subject to photodiodes characterized by a narrow FoV, which may require CPCs structures (see Fig. 2).

B. PROPAGATION MODEL IN VLC

For indoor VLC, the signal propagation comprises two components, the line-of-sight (LoS) channel given by the direct link between optical AP and user, and the non-LoS (NLoS) channel generated by the reflections of the optical

[1]Since the distance between photodiodes of each ADR is much smaller than the distance between optical AP and user, the same irradiance angle can be assumed for all the photodiodes of user k.

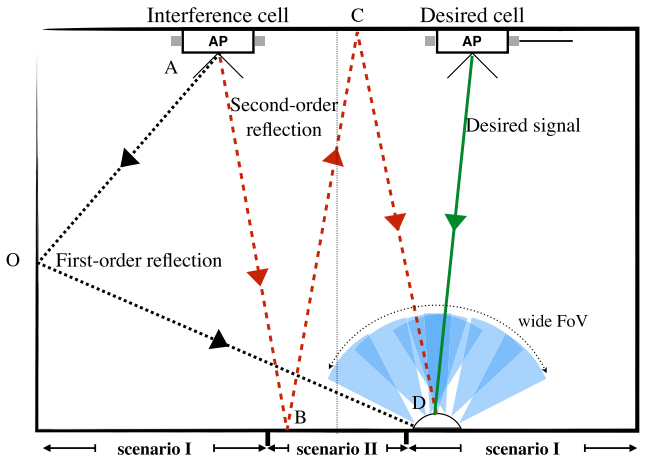

FIGURE 5. Propagation Model for LoS and NLoS signals considering the two regions R_{I} and R_{II}.

signal on walls, floor and ceiling. The resulting optical channel is given by the sum of both components

$$H = H_{\mathrm{LoS}} + H_{\mathrm{NLoS}}, \tag{5}$$

where H_{LoS} and H_{NLoS} is the LoS and NLoS contributions, respectively.

1) LOS CHANNEL

The LoS component follows the Lambertian model, in which the optical channel is defined as DC gain [24]. Omitting the transmitter, receiver and photodiode indexes for the sake of simplicity, the LoS component is given by

$$H_{\mathrm{LoS}} = \begin{cases} \dfrac{(m+1)A\tau}{2\pi d^2}\cos^m(\varphi)T_s(\psi)\cos(\psi) & 0 \le \psi \le \Psi \\ 0 & \text{elsewhere}, \end{cases} \tag{6}$$

where A and τ are the detection area and responsivity of the photodiode, respectively, d is the distance from the optical AP to the user, φ is the angle of irradiance, ψ is the angle of incidence and Ψ is the receiver FoV. The gain of the optical filter plus concentrator is referred to as $T_s(\psi)$. Moreover, in (6), m is the order of Lambertian emission defined by transmitter semi-angle at half power $\varphi_{1/2}$, which is given by

$$m = -\frac{\ln 2}{\ln\cos\left(\varphi_{1/2}\right)}. \tag{7}$$

2) NLOS CHANNEL

The simplified NLoS propagation model for VLC attocells proposed in [19] is considered in this work. This model was validated in [25]. It is basically based on the second-order reflections between points A, B, C, and D as it is shown in Fig. 5. According to [19], this model can be divided into two parts; part 1 (A → B → C) and part 2 (C → D).

In part 1 (A → B → C), the optical signals are transmitted from the light source to point B, and then, they are reflected back to point C. For the considered path, the optical power density can be estimated by

$$\mathcal{I}_0 = \frac{P_{\mathrm{t}}\xi_{\mathrm{floor}}\xi_{\mathrm{ceiling}}(m+1)(n+1)}{2\pi h^2(m+n+4)}, \tag{8}$$

where ξ_{floor} and ξ_{ceiling} are the reflection coefficients from the floor and ceiling given by 0.2 and 0.8, respectively [26]. P_{t}, h represent the transmitted power and height, whereas n the refractive index. Besides, an attenuation factor denoted by λ is introduced so that the resulting power density is

$$\mathcal{I}_v = \mathcal{I}_0\left(\frac{2h}{\sqrt{v^2+4h^2}}\right)^{\lambda}, \tag{9}$$

where v is the horizontal distance from an arbitrary point to point A and λ is attenuation factor to reduce the differences between the conventional and the simplified model [19].

In part 2 (C → D), the optical signals are reflected from the ceiling to the user. Notice that not all reflected signals are received by the photodiodes of each user, since narrow FoV potentially rejects the interfering signals. If the distance between the interfering optical AP and the desired optical AP is $\sqrt{3}R_{\mathrm{cell}}$, where R_{cell} is the cell radius, the NLoS component can be calculated by

$$\mathcal{I}^{\mathrm{NLoS}}(\Psi_{\mathrm{single}}) = N_{\mathrm{AP}}\left[\int_0^{h\tan(\Psi_{\mathrm{single}})}\mathcal{I}_v 2\pi r' H(r')\,\mathrm{d}r'\right]^2, \tag{10}$$

where N_{AP} is the number of neighbouring optical APs. This procedure is illustrated in Fig. 6 for $N_{\mathrm{AP}} = 4$. Then, after integrating all the NLoS components,

$$\mathcal{I}^{\mathrm{NLoS}}(\Psi_{\mathrm{single}}) = N_{\mathrm{AP}}\left[\mathcal{I}_v A T_s(\psi)g(\psi)\left(\cos^{m+1}(\Psi_{\mathrm{single}}) - 1\right)\right]^2\Big|_{v=\sqrt{3}R_{\mathrm{cell}}}, \tag{11}$$

where Ψ_{single} is the FoV of the single-PD receiver. It is worth noticing from this equation that $\mathcal{I}^{\mathrm{NLoS}}(\Psi_{\mathrm{single}})$ is directly affected by FoV.

According to the second-reflection model, the NLoS component is mainly received in the inner cell of the neighbouring optical APs even for wide FoVs as occurs for ADRs (see Fig. 5). This assumption has been considered in previous works such as [19] and [27]. It is worth remarking that other reflection models are available in the state of the art, e.g., [14], [22]. In this sense, the second-order model is assumed for comparison purposes with works such as [19]. On the other hand, other models can be applied straightforwardly.

III. SINR FOR SINGLE-PD RECEIVER

This section is devoted to presenting the statistical distribution of the SINR for single-PD architecture for illustrative purposes. It follows a similar approach as in [19]. In this sense, the narrow FoV of each photodiode that compose the ADR can reject not only the intercell interference but also the first order reflection from wall, particularly for users located

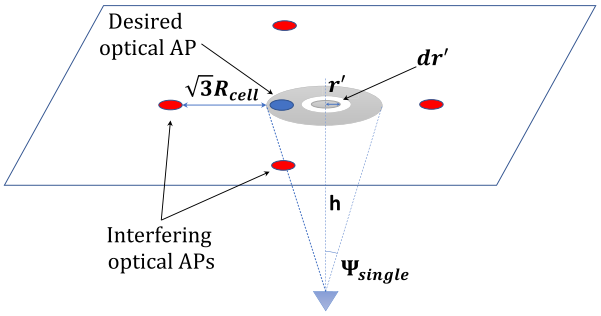

FIGURE 6. Simplified NLoS model part 2 with four interfering optical APs, optical signals reflected from the ceiling.

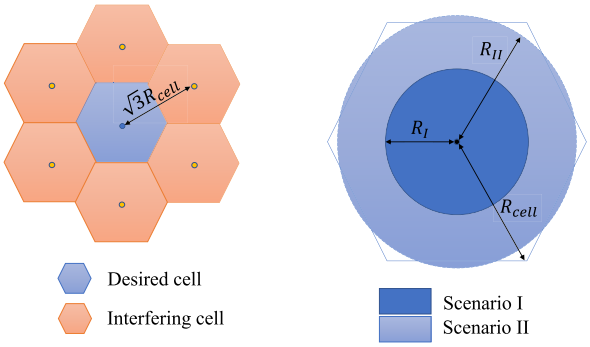

(a) Desired and interfering optical APs, and the regions of scenario I and scenario II.

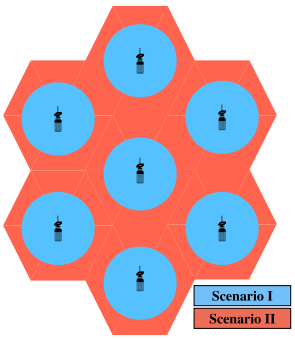

(b) Interference limited network.

FIGURE 7. Division of the attocell network into scenario I and scenario II.

around the cell center. Therefore, the coverage footprint can be divided into high and low SINR regions. This approach has been widely considered in cellular networks based on both RF and optical transmission. Specifically, in [28] and [29], it is demonstrated that the intercell interference can be considered negligible so that the distortion sources are mainly given by noise and other effects such as the NLoS contributions. On the other hand, users at the cell edges are limited by intercell interference making the effects of noise and other sources of distortion negligible. That is, the VLC network is limited by intercell interference in the cell edges while the inner cell is mainly subject to noise and other distortion effects such as the NLoS contribution as it is shown in Fig. 7(b). It is worth remarking that these assumptions have been widely employed for proposing fractional FR (FFR) in small cell networks, e.g., [28] and [29], which recall that require additional frequency bands as well as frequency switching every few meters when applied to VLC networks.

In the following, the coverage footprint of each optical AP is divided into two scenarios; **scenario I** where the intercell interference is mainly given by the diffuse component so that the LoS contribution of the interference can be treated as noise and **scenario II**, which corresponds to the attocell edge, where the intercell interference is mainly given by the LoS contribution, and therefore, considering the NLoS contribution negligible. The relation that defines both regions can be approximated to $R_{\text{II}} \approx 0.91 R_{\text{cell}}$ as proposed in [19]. In the following, the PDF and the CDF in each of these scenarios are calculated.

1) SCENARIO I ($0 \leq R \leq R_{\text{I}}$)

In this scenario, the users are uniformly distributed in an area around the cell center. It is assumed that the interference is mainly generated by the NLoS component while the intercell interference from the LoS component can be considered negligible. Then, the interference follows the model described in subsection II-B2. The coverage area of scenario I is defined by a radius $r \leq R_{\text{I}}$, where R_{I} is the bound that defines this region. Thus, the PDF of the radius that defines scenario I is given by,

$$f_{\text{I}}(r) = \frac{2r}{R_{\text{I}}^2}, \quad (0 \leq r \leq R_{\text{I}}). \tag{12}$$

For the single-PD architecture, the distance and cosine of the irradiance and incidence angles can be determined straightforwardly as $d = (r^2 + h^2)^{1/2}$, $\cos(\varphi) = h/(r^2 + h^2)^{1/2}$, and $\cos(\psi) = h/(r^2 + h^2)^{1/2}$. By substituting these parameters in (6), the channel gain of single-PD architecture can be written as

$$H(r, \Psi_{\text{single}}) = \frac{C(m+1)h^{(m+1)}}{(r^2 + h^2)^{\frac{m+3}{2}}}, \tag{13}$$

where recall that h is the height from optical AP to users and C is given by

$$C = \frac{1}{2\pi} A \tau T_s(\psi) g(\psi). \tag{14}$$

It is worth remarking that, the channel gain obtained in (13) is only valid for the single-PD architecture. Notice that the same derivation cannot be considered for ADRs since the photodiodes follow a specific orientation. Considering the NLoS interference as the main contribution of signal distortion, the noise can be negligible. Then, the SINR of the single-PD architecture is given by

$$\gamma(r) = \frac{(P_{\text{t}} H(r, \Psi_{\text{single}}))^2}{\mathcal{I}^{\text{NLoS}}(\Psi_{\text{single}}) + \sigma_n^2} \approx \frac{(P_{\text{t}} H(r, \Psi_{\text{single}}))^2}{\mathcal{I}^{\text{NLoS}}(\Psi_{\text{single}})}. \tag{15}$$

Applying the change of variable method, the PDF function of the SINR can be calculated as

$$f_\gamma(\gamma) = \left| \frac{\partial}{\partial \gamma} u^{-1}(\gamma) \right| \cdot f_{\text{I}} \left(u^{-1}(\gamma) \right), \tag{16}$$

where u^{-1} is the inverse function of u. The PDF of the SINR for single-PD in the region ($r \leq R_{\mathrm{I}}$) can be expressed by

$$f_{\mathrm{I}}(\gamma) = \begin{cases} \dfrac{h^2}{(m+3)R_{\mathrm{I}}^2}\gamma_0^{\frac{1}{m+3}}\gamma^{-\frac{m+4}{m+3}} & \gamma_{\mathrm{I}} \leq \gamma \leq \gamma_0 \\ 0 & \text{otherwise,} \end{cases} \tag{17}$$

where γ_0, and γ_{I} are the maximum and minimum SINR at the cell center, $r = 0$, and at the edge of the region, $r = R_{\mathrm{I}}$, respectively, which are given by

$$\gamma_0 = \frac{\left(P_{\mathrm{t}}H(0, \Psi_{\mathrm{single}})\right)^2}{\mathcal{I}^{\mathrm{NLoS}}(\Psi_{\mathrm{single}})}, \tag{18}$$

$$\gamma_{\mathrm{I}} = \frac{\left(P_{\mathrm{t}}H(R_{\mathrm{I}}, \Psi_{\mathrm{single}})\right)^2}{\mathcal{I}^{\mathrm{NLoS}}(\Psi_{\mathrm{single}})}. \tag{19}$$

Then, by integrating (17), the CDF of SINR in scenario I can be derived as

$$F_{\mathrm{I}}(\gamma) = \begin{cases} 0 & \gamma < \gamma_{\mathrm{I}} \\ \dfrac{h^2}{R_{\mathrm{I}}^2}\gamma_0^{\frac{1}{m+3}}\left(\gamma_{\mathrm{I}}^{-\frac{1}{m+3}} - \gamma^{-\frac{1}{m+3}}\right) & \gamma_{\mathrm{I}} \leq \gamma \leq \gamma_0 \\ 1 & \gamma > \gamma_0. \end{cases} \tag{20}$$

2) SCENARIO II ($R_{\mathrm{I}} \leq R \leq R_{\mathrm{II}}$)

In this scenario, the users are located in the edge of the attocell where the main contribution of the interference is given by the LoS component. Then, the contribution of the NLoS component can be considered negligible. The scenario II is defined by the bounds $R_{\mathrm{I}} < r \leq R_{\mathrm{II}}$, where R_{II} defines the limit of the coverage footprint generated by the optical AP as it is shown in Fig. 7(a). Then, the PDF of the radius that defines scenario II is given by

$$f_{\mathrm{II}}(r) = \frac{2r}{R_{\mathrm{II}}^2 - R_{\mathrm{I}}^2}, \quad (R_{\mathrm{I}} \leq r \leq R_{\mathrm{II}}). \tag{21}$$

Since the interference from the NLoS component is negligible, the SINR exclusively consider the intercell interference received from the LoS contributions. Then, the SINR in this scenario can be approximated as proposed in [19],

$$\gamma(r) \approx \left(\frac{h^2 + \tilde{r}_{l'}^2}{h^2 + (\sqrt{3}R_{\mathrm{cell}} - r)^2}\right)^{-(m+3)}, \tag{22}$$

where $\tilde{r}_{l'} = \sqrt{3}R_{\mathrm{cell}} - (R_{\mathrm{I}} + R_{\mathrm{II}})/2$. Then, by applying the change-of-variable method, the PDF of the SINR in this scenario is

$$f_{\mathrm{II}}(\gamma) = \begin{cases} \dfrac{h^2 + \tilde{r}_{l'}^2}{(m+3)(R_{\mathrm{II}}^2 - R_{\mathrm{I}}^2)}\gamma^{-\frac{m+2}{m+3}} & 1 \leq \gamma \leq \gamma'_{\mathrm{I}} \\ 0 & \text{otherwise,} \end{cases} \tag{23}$$

After integrating the PDF, the CDF of SINR is given by

$$F_{\mathrm{II}}(\gamma) = \begin{cases} 0 & \gamma < 1 \\ \dfrac{h^2 + \tilde{r}_{l'}^2}{R_{\mathrm{II}}^2 - R_{\mathrm{I}}^2}\left(-1 + \gamma^{\frac{1}{m+3}}\right) & 1 \leq \gamma \leq \gamma'_{\mathrm{I}} \\ 1 & \gamma > \gamma'_{\mathrm{I}}, \end{cases} \tag{24}$$

where γ'_{I} represents the SINR in the boundary region at $r = R_{\mathrm{I}}$, and it can be calculated by

$$\gamma'_{\mathrm{I}} = \left(\frac{h^2 + \tilde{r}_{l'}^2}{h^2 + (\sqrt{3}R_{\mathrm{cell}} - R_{\mathrm{I}})^2}\right)^{-(m+3)}. \tag{25}$$

3) OVERALL THEORETICAL SINR ($0 \leq R \leq R_{\mathrm{II}}$)

To determine the overall performance for single-PD architecture, the derivation of the PDF of SINR for both scenarios must be combined. The PDF function of r in the entire coverage footprint of optical AP is given by

$$f_{\mathrm{O}}(r) = \frac{2r}{R_{\mathrm{II}}^2}, \quad (0 \leq r \leq R_{\mathrm{II}}). \tag{26}$$

The two SINR scenarios can be also defined as high-SINR and low-SINR regions. In the high-SINR region, which is associated to scenario I, users equipped with a narrow FoV photodiode can effectively reject the LoS component of the interference from neighboring cells, leaving only NLoS interference, and therefore, achieving high SINRs. On the other hand, in the low-SINR region, which is associated to scenario II, the users receive the LoS component of the intercell interference. It is worth noting that the transition from high to low SINR regions is very sharp due to the FoV-limited optical receiver, which creates a cut-off effect.

So, according to [19], the overall PDF and CDF of the SINR can be written as

$$f_{\mathrm{O}}(\gamma) = \begin{cases} \dfrac{R_{\mathrm{II}}^2 - R_{\mathrm{I}}^2}{R_{\mathrm{II}}^2}f_{\mathrm{II}}(\gamma) & 1 \leq \gamma \leq \gamma'_{\mathrm{I}} \\ \dfrac{R_{\mathrm{I}}^2}{R_{\mathrm{II}}^2}f_{\mathrm{I}}(\gamma) & \gamma_{\mathrm{I}} \leq \gamma \leq \gamma_0 \\ 0 & \text{otherwise.} \end{cases} \tag{27}$$

$$F_{\mathrm{O}}(\gamma) = \frac{R_{\mathrm{I}}^2}{R_{\mathrm{II}}^2}F_{\mathrm{I}}(\gamma) + \frac{R_{\mathrm{II}}^2 - R_{\mathrm{I}}^2}{R_{\mathrm{II}}^2}F_{\mathrm{II}}(\gamma), \tag{28}$$

where $f_{\mathrm{O}}(\gamma)$, $F_{\mathrm{O}}(\gamma)$ are the overall PDF and CDF of the SINR for the single-PD over whole region.

IV. COMBINING ADR SCHEMES IN VLC

This work is focused on exploiting the concept of ADRs in attocell optical networks. The main idea behind the ADRs is to maximize the SINR of the users. In this section, we present a brief review of the photodiode combining schemes that can be applied exploiting the concept of ADR. Furthermore, it is assumed that each user is connected to the optical AP that

provides the strongest signal. That is,

$$l_d = \arg\max_{l} \left\{ \sum_{i=1}^{N_{\text{PD}}} |H_{l,i}|^2 \right\}, \tag{29}$$

where l_d is the index of the desired AP.

In the following, the SBC, EGC and MRC photodiode combination schemes are described in detail [19].

A. SELECT BEST COMBINING (SBC)

For SBC scheme, the photodiode of the ADR that maximizes the SINR from the set of possible photodiodes is selected. Then, the optical link is given by the desired AP and the selected photodiode. Mathematically, the selection of AP and photodiodes for SBC can be formulated as

$$\{l_d, \text{PD}_\text{s}\} = \arg\max_{l,i} \left\{ \gamma_{(l,i)} \right\}, \tag{30}$$

where l_d is the desired optical AP and PD_s is the selected PD. Then, the SINR between the AP l and PD i is given by

$$\gamma_{(l,i)} = \frac{\left(P_\text{t} H_{(l,i)}\right)^2}{\sum\limits_{l'=1,l'\neq l}^{L} \left(P_\text{t} H_{(l',i)}\right)^2 + \sigma_n^2}. \tag{31}$$

B. EQUAL GAIN COMBINING (EGC)

In contrast to SBC, for EGC all the photodiodes of the ADR are selected and the received signal is multiplied by an equal weight for all of them. Notice that, the sum of the optical power received by photodiodes that compose the ADR is much higher than the optical power received by SBC. However, receiving the optimal signal from all the possible orientation of the ADR involves a interference level much greater that for SBC, which rejects the interference from the non-selected photodiodes.

$$\gamma_{(l,k)} = \frac{\left(\sum\limits_{i=1}^{N_{\text{PD}}} P_\text{t} H_{(l,i)}\right)^2}{\sum\limits_{l'=1,l'\neq l}^{L} \left(P_\text{t} \sum_{i=1}^{N_{\text{PD}}} H_{(l',i)}\right)^2 + N_{\text{PD}}\sigma_n^2}. \tag{32}$$

C. MAXIMUM RATIO COMBINING (MRC)

For the MRC scheme, different weights are assigned to each of the photodiodes of the ADR in order to maximize the SINR. Then, it can exploit the signal received by each photodiodes while minimizing, or even canceling, the effect of the photodiodes subject to strong levels of interference. Therefore, MRC achieves a higher SINR compared to SBC and EGC schemes. However, notice that it requires CSI to calculate the weights that maximize the SINR. Specifically, the SINR achieved by the MRC scheme can be written as

$$\gamma_{(l,k)} = \frac{\left(\sum\limits_{i=1}^{N_{\text{PD}}} P_\text{t} w_{(l,i)} H_{(l,i)}\right)^2}{\sum_{l'=1,l'\neq l}^{L} \left(P_\text{t} \sum\limits_{i=1}^{N_{\text{PD}}} w_{(l,i)} H_{(l',i)}\right)^2 + \sum_{i=1}^{N_{\text{PD}}} w_{(l,i)}^2 \sigma_n^2}, \tag{33}$$

where the weights are denoted by $w_{(l,i)}$ and they can be determined as

$$w_{(l,i)} = \frac{\left(P_\text{t} H_{(l,i)}\right)^2}{\sum_{l'=1,l'\neq l}^{L} \left(P_\text{t} H_{(l',i)}\right)^2 + \sigma_n^2}. \tag{34}$$

Remark 1: Notice that there exist more complex schemes such as optimum combining (OPC) [30] or transmit precoding schemes based on maximizing the signal space [21] that exploit the channel correlation matrix generated by the ADRs subject to obtaining global CSI. Analyzing these schemes requires to consider issues such as pilot transmission, channel estimation and updating, etc. For the sake of simplicity, this work is focused on the described schemes, SBC, EGC and MRC since they provide an intuitive overview of the impact of overlapping FoV ADRs in VLC, which can be extended to other more complex transmission schemes.

V. SINR FOR ANGLE DIVERSITY RECEIVERS

The statistical characterization of single-PD architecture described above can be derived straightforwardly based on the closed-form of the channel obtained in (13). However, this methodology cannot be applied to ADRs since the cosine of the incidence angle depends on the orientation of each photodiode as well as the radius and height that define the location of the user. In the following, we derive the statistical characterization of the SINR for SBC, EGC and MRC for ADRs composed by overlapping FoV photodiodes. For the sake of simplicity, we assume that the ADRs follow a pyramidal arrangement. The extension to other arrangements can be obtained straightforwardly.

In this section, a similar approach based on dividing the coverage footprint into scenario I and II is assumed. In the inner cell (scenario I) the intercell interference can be considered negligible, which may result more noticeable due to the angular diversity provided by the ADR, so that the sources of distortion are given by the noise and the NLoS contribution according to the second-order reflection model [19]. In scenario II the users are mainly limited by intercell interference, which results much greater that other sources of distortion such as noise or interference from reflections. In [25], it is demonstrated that even for the wide FoV generated by ADRs the first-order reflection can be rejected (see Fig. 5) while the second-order reflection is received in the inner cell of neighbouring cells (scenario I). In contrast to previous works such as [19], in the following we assume an overlapping FoVs ADR so that multiple photododiodes may receive LoS contributions. Notice that

a closed-form of the incidence angle (see (13)) cannot be obtained, which hampers the derivation of the PDF and CDF applying the change of variable method described in Section III (see (16)).

A. SINR FOR SBC SCHEME

As previously discussed, SBC selects a single photodiode while rejecting the signal (or interference) from all other photodiodes. Therefore, increasing the number of photodiodes that compose the ADR, i.e., each with a narrow FoV, leads to improving the efficiency of the interference rejection. In other words, for ADRs equipped with a large number of photodiodes, there exists at least a photodiode with a similar orientation as the vector between user and optical AP of interest, which provides an incidence angle close to zero, almost surely. Therefore, the following assumption can be formulated,

Assumption 1: For an ADR composed of enough photodiodes,

$$\exists\, i \in \{1, \ldots, N_P\} : \ \cos(\psi_{l,i}) = (1 - \epsilon) \approx 1, \tag{35}$$

where $\psi_{l,i}$ is the incidence angle between optical AP l and photodiode i of the user of interest and ϵ is a value small enough to satisfy the condition $\cos(\psi_{l,i}) \approx 1$.

In order to validate the proposed assumption, we analyze the cosine of the incidence angle of the selected photodiode for SBC as the number of photodiodes of the ADR increases through Monte Carlo simulations in an attocell with a radius $R_{\text{cell}} = 3$ m in Fig. 8. It can be seen that the condition $\epsilon \leq 0.1$ is achieved for ADRs equipped with $N_{\text{PD}} = 4$ or more photodiodes. Besides, increasing the number of photodiodes to a reasonable value, e.g., $N_{\text{PD}} = 8$, obtains a condition $\epsilon \leq 0.05$ for an elevation angle equal to 30° in the proposed pyramidal arrangement. To fully characterize the impact of the incidence angle in ADRs, the CDF of these parameters is depicted in Fig. 9 for a pyramidal ADR with an elevation angle equal to 30° and $N_{\text{PD}} = 6$ photodiodes. It can be seen that the cosine of the incidence angle takes value above 0.9 ($\epsilon = 0.1$) in approximately 94% of the cases.

Similarly to the methodology employed in Section III for single-PD architecture, the coverage footprint of each optical AP is divided into scenario I and II, in which the intercell interference are mainly generate because of the NLoS and LoS components, respectively.

1) SCENARIO I ($0 \leq R \leq R_{\text{I}}$)

For scenario I, the interference is mainly given by the NLoS component. Then, the SINR obtained by SBC is given by

$$\gamma(r)_{\text{SBC}} = \frac{(P_{\text{t}} H(r, \Psi_{\text{ADR}}))^2}{\mathcal{I}^{\text{NLoS}}(\Psi_{\text{ADR}}) + \sigma_n^2} \approx \frac{(P_{\text{t}} H(r, \Psi_{\text{ADR}}))^2}{\mathcal{I}^{\text{NLoS}}(\Psi_{\text{ADR}})}, \tag{36}$$

where $\mathcal{I}^{\text{NLoS}}(\Psi_{\text{ADR}})$ is the interference from the NLoS contribution received by the selected photodiode and $H(r, \Psi_{\text{ADR}})$ is the channel for the selected photodiode.

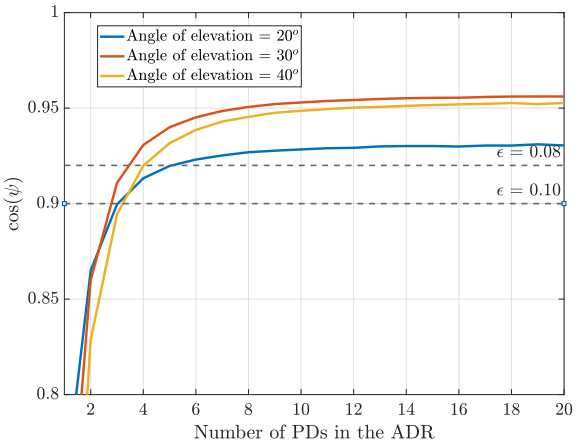

FIGURE 8. The incident of angle $\cos(\psi_I)$ with respects to the number of the PDs at different elevation angles.

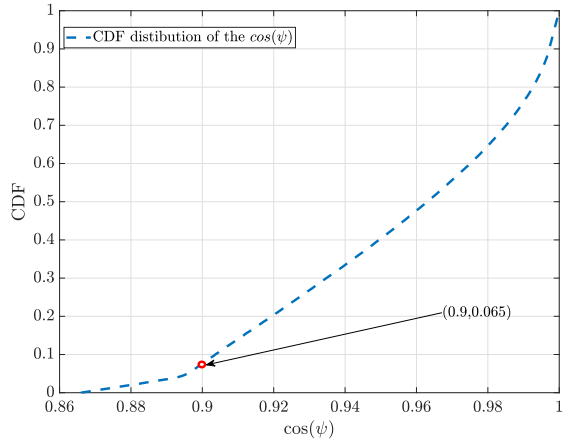

FIGURE 9. The CDF of the incident of angle $\cos(\psi_I)$, with elevation angle = 30°.

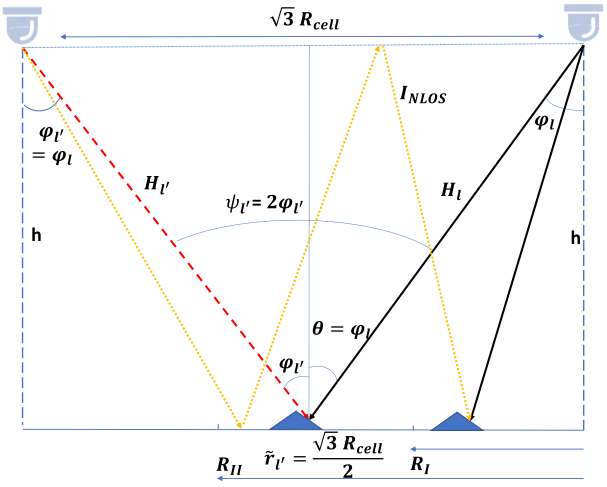

FIGURE 10. Scenario I and II for SBC, the desired and the interfering signals. H_I is the desired signal, $H_{I'}$ is the interfering LoS signal and I_{NLoS} is NLoS interference.

Applying (35), this channel can be written as

$$H(r, \Psi_{\text{ADR}}) = \frac{C(m+1)h^m}{(r^2 + h^2)^{\frac{m+2}{2}}}. \tag{37}$$

Then, using the change of variable method, the PDF of the SINR is given in (38), as shown at the bottom of the next page, where $\gamma_{0.\mathrm{SBC}}$ is the maximum SINR, which is obtained for $r = 0$, i.e.,

$$\gamma_{0.\mathrm{SBC}} = \frac{\left(P_{\mathrm{t}} H(0, \Psi_{\mathrm{ADR}})\right)^2}{\mathcal{I}^{\mathrm{NLoS}}(\Psi_{\mathrm{ADR}})}, \tag{39}$$

and $\gamma_{\mathrm{I.SBC}}$ is the minimum SINR corresponding to $r = R_{\mathrm{I}}$,

$$\gamma_{\mathrm{I.SBC}} = \frac{\left(P_{\mathrm{t}} H(R_{\mathrm{I}}, \Psi_{\mathrm{ADR}})\right)^2}{\mathcal{I}^{\mathrm{NLoS}}(\Psi_{\mathrm{ADR}})}. \tag{40}$$

Integrating the PDF equation, the CDF of the SINR for scenario I is given in equation (41), as shown at the bottom of the next page.

2) SCENARIO II ($R_{\mathrm{I}} \leq R \leq R_{\mathrm{II}}$)

In this scenario, the signal and interfering contributions correspond to the LoS components denoted by $H_l(r)$ and $H_{l'}(r)$, respectively. Similarly to scenario I, it is assumed that the selected photodiode of the ADR satisfies the condition (35) for the selected optical AP that provides the signal link. For the interfering link, the contribution is bounded to the attocell edge, in which the interference in maximized, given by the point $\tilde{r}_{l'} = \sqrt{3} R_{\mathrm{cell}}/2$.

Assumption 2: Around scenario II, the irradiance angles of the optical APs satisfy the condition $\varphi_l \approx \varphi_{l'}$, where φ_l and $\varphi_{l'}$ are the irradiance angles of the intended and interfering optical APs, respectively. Since according to assumption 1 the orientation of the selected photodiode is perpendicular to the desired optical AP, the incident angle of the interfering link is given by $\psi_{l'} \approx 2\varphi_{l'}$ as it is shown in Fig. 10. This assumption is validated through Monte Carlo simulations in Fig. 11. It can be seen that the cosine of the incidence angle is bounded by the values obtained using the proposed assumption.

Applying, this geometrical assumption, the SINR in this scenario can be approximated as

$$\gamma(r)_{\mathrm{SBC}} \approx \frac{(h^2 + \tilde{r}_{l'}^2)^{m+4}}{(h^2 + r^2)^{m+2}(h^2 - \tilde{r}_{l'}^2)^2}. \tag{42}$$

Then, the PDF of SINR for this scenario can be derived. After some mathematical rearrangement, the PDF is given in (43), as shown at the bottom of page 12, where $\gamma'_{\mathrm{I.SBC}}$ is the SINR at the boundary region at $r = R_{\mathrm{I}}$,

$$\gamma'_{\mathrm{I.SBC}} = \frac{(h^2 + \tilde{r}_{l'}^2)^{m+4}}{(h^2 + R_{\mathrm{I}}^2)^{m+2}(h^2 - \tilde{r}_{l'}^2)^2}, \tag{44}$$

and $\gamma_{\mathrm{II.SBC}}$ is the SINR for $r = R_{\mathrm{II}}$ given by

$$\gamma_{\mathrm{II.SBC}} = \frac{(h^2 + \tilde{r}_{l'}^2)^{m+4}}{(h^2 + R_{\mathrm{II}}^2)^{m+2}(h^2 - \tilde{r}_{l'}^2)^2}. \tag{45}$$

Then, by integrating the PDF, the CDF of the SINR is given in (46), as shown at the bottom of page 12.

3) OVERALL THEORETICAL SINR ($0 \leq R \leq R_{\mathrm{II}}$)

The overall performance of SINR for SBC scheme is derived from the scenario I and II based on the overall PDF of r in (see (26)). So, the overall PDF of the SINR is given by

$$f_{\mathrm{O}}(\gamma)_{\mathrm{SBC}} = \begin{cases} \dfrac{R_{\mathrm{II}}^2 - R_{\mathrm{I}}^2}{R_{\mathrm{II}}^2} f_{\mathrm{II}}(\gamma)_{\mathrm{SBC}} & \gamma_{\mathrm{II.SBC}} \leq \gamma \leq \gamma'_{\mathrm{I.SBC}} \\ \dfrac{R_{\mathrm{I}}^2}{R_{\mathrm{II}}^2} f_{\mathrm{I}}(\gamma)_{\mathrm{SBC}} & \gamma_{\mathrm{I.SBC}} \leq \gamma \leq \gamma_{0.\mathrm{SBC}} \\ 0 & \text{otherwise,} \end{cases} \tag{47}$$

Applying (41) and (46), the overall CDF of the SINR for SBC scheme is given by

$$F_{\mathrm{O}}(\gamma)_{\mathrm{SBC}} = \frac{R_{\mathrm{I}}^2}{R_{\mathrm{II}}^2} F_{\mathrm{I}}(\gamma)_{\mathrm{SBC}} + \frac{R_{\mathrm{II}}^2 - R_{\mathrm{I}}^2}{R_{\mathrm{II}}^2} F_{\mathrm{II}}(\gamma)_{\mathrm{SBC}}. \tag{48}$$

B. SINR FOR EGC SCHEME

For the EGC scheme, the signal and interference are received by all the photodiodes that compose the ADR. Then, each photodiode is characterized by a distinct incidence angle.

1) SCENARIO I ($0 \leq R \leq R_{\mathrm{I}}$)

First, we characterize the incidence angle for all the photodiodes that compose the ADR. Omitting the photodiode index for the sake of simplicity, the incidence angle of a generic photodiode for optical AP l can be written as

$$\cos(\psi_l) = \frac{1}{d_l}\left[(x_l - x)\cos(\alpha)\sin(\theta) + (y_l - y)\sin(\alpha)\sin(\theta) + (z_l - z)\cos(\theta)\right]. \tag{49}$$

$$\overset{(a)}{=} \frac{1}{d_l}\left[r\cos(\beta_l)\cos(\alpha)\sin(\theta) + r\sin(\beta_l)\sin(\alpha)\sin(\theta) + h\cos(\theta)\right]. \tag{50}$$

where d_l is the distance to optical AP l, $[x_l, y_l, z_l]$ is the position of the optical AP, and $[x, y, z]$ is the position of the user. Recall that α and θ are the azimuthal and elevation angles of the photodiode, respectively. The step (a) introduces the parameter β_l defined as the angle in the (x-y) plane between the optical AP and the user. Assuming that the condition (35) is satisfied, i.e., $\cos(\psi_l) = 1$, it can be checked that $\beta_l = 0$, where l is the optical AP of interest. Additionally, the elevation angle θ is equal to the angle of irradiance on that face as illustrated in Fig. 10. Then, $\cos(\theta) = h/\sqrt{(h^2 + r^2)}$ and $\sin(\theta) = r/\sqrt{(h^2 + r^2)}$. Subsequently, the incident angles of the other photodiodes can be calculated based on their azimuthal angle and the incident angle of the first photodiode. Thus, the incident $\psi_{l,i}$ of the i-th photodiode can be determined as

$$\cos(\psi_{l,i}) = \frac{1}{d_l^2}(r^2\cos(\alpha_i) + h^2), \tag{51}$$

where $\alpha_i = 2(i-1)\pi/N_{\mathrm{PD}}$.

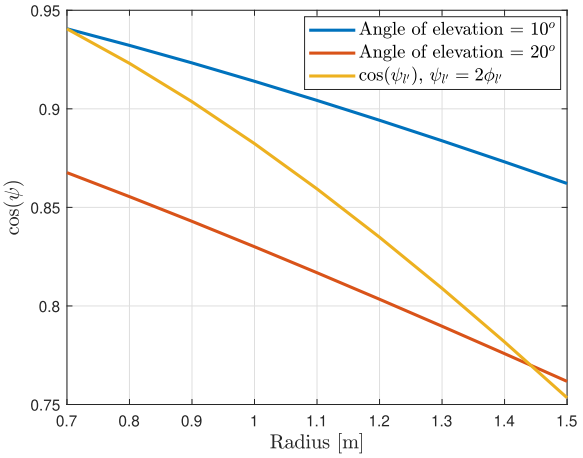

FIGURE 11. Cosine of incident angle of the interfering link $\psi_{l'} \approx 2\varphi_{l'}$ in scenario 2 ($R1 < r < R2$).

Therefore, the channel gain $H_{l,i}(r, \Psi_{\text{ADR}})$ from the optical AP l to the i-th photodiode for the EGC scheme can be written as

$$H_{l,i}(r, \Psi_{\text{ADR}}) = \frac{C(m+1)\cos^m(\varphi)\cos(\psi_{l,i})}{d_l^2}. \tag{52}$$

For the sake of an easy explanation, let us introduce the following expression for the cosine of the incidence angle,

$$\cos(\psi_{l,i}) = \frac{Q_{l,i}}{d_l^2} = \frac{\tilde{r}_{l,I}^2\cos(\alpha_i) + h^2}{d_l^2}, \tag{53}$$

where $Q_{l,i} = \tilde{r}_{l,I}^2\cos(\alpha_i) + h^2$, and $\tilde{r}_{l,I} = R_{\text{I}}/2$. Then, the channel gain $H_{l,i}(r, \Psi_{\text{ADR}})$ of the i-th photodiode can be written as

$$H_{l,i}(r, \Psi_{\text{ADR}}) = \frac{C(m+1)h^m Q_{l,i}}{(r^2+h^2)^{\frac{m+2}{2}}}. \tag{54}$$

Then, the SINR for scenario I in EGC scheme is

$$\gamma(r)_{\text{EGC}} = \frac{\left(P_{\text{t}}\sum_{i=1}^{N_{\text{PD}}} H_{l,i}(r, \Psi_{\text{ADR}})\right)^2}{\sum_{i=1}^{N_{\text{PD}}} \mathcal{I}_i^{\text{NLoS}}(\Psi_{\text{ADR}}) + \sigma_n^2} \approx \frac{\left(P_{\text{t}}\sum_{i=1}^{N_{\text{PD}}} H_{l,i}(r, \Psi_{\text{ADR}})\right)^2}{\sum_{i=1}^{N_{\text{PD}}} \mathcal{I}_i^{\text{NLoS}}(\Psi_{\text{ADR}})}. \tag{55}$$

Therefore, applying the change of variable method and after some mathematical rearrangement the PDF of SINR for EGC in scenario I is given in (56), as shown at the bottom of the next page, where $\gamma_{0.\text{EGC}}$ is the maximum SINR, which occurs at $r = 0$, i.e.,

$$\gamma_{0.\text{EGC}} = \frac{\left(P_{\text{t}}\sum_{i=1}^{N_{\text{PD}}} H_{l,i}(0, \Psi_{\text{ADR}})\right)^2}{\sum_{i=1}^{N_{\text{PD}}} \mathcal{I}_i^{\text{NLoS}}(\Psi_{\text{ADR}})}, \tag{57}$$

and $\gamma_{\text{I.EGC}}$ is the minimum SINR for $r = R_{\text{I}}$, which is given by

$$\gamma_{\text{I.EGC}} = \frac{\left(P_{\text{t}}\sum_{i=1}^{N_{\text{PD}}} H_{l,i}(R_{\text{I}}, \Psi_{\text{ADR}})\right)^2}{\sum_{i=1}^{N_{\text{PD}}} \mathcal{I}_i^{\text{NLoS}}(\Psi_{\text{ADR}})}. \tag{58}$$

Then, integrating the PDF derived in (56), the CDF of SINR for scenario I is given in (59), as shown at the bottom of the next page.

2) SCENARIO II ($R_{\text{I}} \le R \le R_{\text{II}}$)

In this case, the interference is mainly given by the LoS component. Similarly to scenario I, the elevation angle satisfies the following conditions $\cos(\theta) = h/\sqrt{(h^2+r^2)}$ and $\sin(\theta) = r/\sqrt{(h^2+r^2)}$. However, for this scenario notice that $\beta_{l'}$ is not zero in order to differentiate $\psi_{l,i}$ and $\psi_{l',i}$, $l' \neq l$.

$$f_{\text{I}}(\gamma)_{\text{SBC}} = \begin{cases} \dfrac{h^2}{(m+2)R_{\text{I}}^2}(\gamma_{0.\text{SBC}})^{\frac{1}{m+2}}\gamma^{-\frac{m+3}{m+2}} & \gamma_{\text{I.SBC}} \le \gamma \le \gamma_{0.\text{SBC}} \\ 0 & \text{otherwise} \end{cases} \tag{38}$$

$$F_{\text{I}}(\gamma)_{\text{SBC}} = \begin{cases} 0 & \gamma < \gamma_{\text{I.SBC}} \\ \dfrac{h^2}{R_{\text{I}}^2}\gamma_{0.\text{SBC}}^{\frac{1}{m+2}}\left(\gamma_{\text{I.SBC}}^{-\frac{1}{m+2}} - \gamma^{-\frac{1}{m+2}}\right) & \gamma_{\text{I.SBC}} \le \gamma \le \gamma_{0.\text{SBC}} \\ 1 & \gamma > \gamma_{0.\text{SBC}} \end{cases} \tag{41}$$

Then, the angle of incidence for the interfering optical APs, $l' \neq l$, and the i-th photodiode can be written as

$$\cos(\psi_{l',i}) = \frac{1}{d_l^2}(r^2\cos(\beta_{l'} - \alpha_i) + h^2). \tag{60}$$

Applying these geometrical derivations, the SINR for EGC in scenario II corresponds to

$$\gamma(r)_{\text{EGC}} \approx \frac{\left(\sum_{i=1}^{N_{\text{PD}}} H_{l,i}(r, \Psi_{\text{ADR}})\right)^2}{\left(\sum_{i=1}^{N_{\text{PD}}} H_{l',i}(\tilde{r}_{l',II}, \Psi_{\text{ADR}})\right)^2} = \frac{\left(\sum_{i=1}^{N_{\text{PD}}} Q_{l,i}\right)^2 (\tilde{r}_{l',II}^2 + h^2)^{4+m}}{\left(\sum_{i=1}^{N_{\text{PD}}} Q_{l',i}\right)^2 (r^2 + h^2)^{4+m}}, \tag{61}$$

where $H_{l,i}(r, \Psi_{\text{ADR}})$ is channel between the desired optical AP l and the photodiode i, $H_{l',i}(\tilde{r}_{l',II}, \Psi_{\text{ADR}})$ is the interfering LoS channel between optical AP l' and the photodiode i. Moreover, in (61), $Q_{l,i} = \tilde{r}_{l',II}^2\cos(\alpha_i) + h^2$, and $Q_{l',i} = \tilde{r}_{l',II}^2\cos(\beta_{l'} - \alpha_i) + h^2$.

Following the methodology employed in the previous scenario, the PDF of SINR in scenario II is given in (64), as shown at the bottom of the next page, where $\gamma'_{\text{I.EGC}}$ and $\gamma_{\text{II.EGC}}$ represent the maximum and minimum SINR in the region at $r = R_{\text{I}}$ and $r = R_{\text{II}}$, respectively. That is,

$$\gamma'_{\text{I.EGC}} = \frac{\left(\sum_{i=1}^{N_{\text{PD}}} Q_{l,i}\right)^2 (\tilde{r}_{l',II}^2 + h^2)^{4+m}}{\left(\sum_{i=1}^{N_{\text{PD}}} Q_{l',i}\right)^2 (R_{\text{I}}^2 + h^2)^{4+m}}, \tag{62}$$

and

$$\gamma_{\text{II.EGC}} = \frac{\left(\sum_{i=1}^{N_{\text{PD}}} Q_{l,i}\right)^2 (\tilde{r}_{l',II}^2 + h^2)^{4+m}}{\left(\sum_{i=1}^{N_{\text{PD}}} Q_{l',i}\right)^2 (R_{\text{II}}^2 + h^2)^{4+m}}. \tag{63}$$

Then, integrating the PDF, the CDF of SINR in scenario II can be written as in (65), as shown at the bottom of the next page.

3) OVERALL THEORETICAL SINR ($0 \leq R \leq R_{\text{II}}$)

Assuming that the users are uniformly distributed in the entire coverage footprint (see (26)), the overall PDF and CDF of SINR for EGC scheme can be written as

$$f_{\text{O}}(\gamma)_{\text{EGC}} = \begin{cases} \frac{R_{\text{II}}^2 - R_{\text{I}}^2}{R_{\text{II}}^2} f_{\text{II}}(\gamma)_{\text{EGC}} & \gamma_{\text{II.EGC}} \leq \gamma \leq \gamma'_{\text{I.EGC}} \\ \frac{R_{\text{I}}^2}{R_{\text{II}}^2} f_{\text{I}}(\gamma)_{\text{EGC}} & \gamma_{\text{I.EGC}} \leq \gamma \leq \gamma_{\text{0.EGC}} \\ 0 & \text{otherwise,} \end{cases} \tag{66}$$

$$f_{\text{II}}(\gamma)_{\text{SBC}} = \begin{cases} \frac{(h^2 + \tilde{r}_{l'}^2)^{\frac{m+4}{m+2}}}{(m+2)(h^2 - \tilde{r}_{l'}^2)^{\frac{2}{m+2}}(R_{\text{II}}^2 - R_{\text{I}}^2)} \gamma^{-\frac{m+3}{m+2}} & \gamma_{\text{II.SBC}} \leq \gamma \leq \gamma'_{\text{I.SBC}} \\ 0 & \text{otherwise} \end{cases} \tag{43}$$

$$F_{\text{II}}(\gamma)_{\text{SBC}} = \begin{cases} 0 & \gamma < \gamma_{\text{II,SBC}} \\ \frac{(h^2 + \tilde{r}_{l'}^2)^{\frac{m+4}{m+2}}}{(h^2 - \tilde{r}_{l'}^2)^{\frac{2}{m+2}}(R_{\text{II}}^2 - R_{\text{I}}^2)} (\gamma_{\text{II.EGC}}^{-\frac{1}{m+2}} - \gamma^{-\frac{1}{m+2}}) & \gamma_{\text{II.SBC}} \leq \gamma \leq \gamma'_{\text{I.SBC}} \\ 1 & \gamma > \gamma'_{\text{I.SBC}} \end{cases} \tag{46}$$

$$f_{\text{I}}(\gamma)_{\text{EGC}} = \begin{cases} \frac{h^2}{(m+4)R_{\text{I}}^2} (\gamma_{\text{0.EGC}})^{\frac{1}{m+4}} \gamma^{-\frac{m+5}{m+4}} & \gamma_{\text{I.EGC}} \leq \gamma \leq \gamma_{\text{0.EGC}} \\ 0 & \text{otherwise} \end{cases} \tag{56}$$

$$F_{\text{I}}(\gamma)_{\text{EGC}} = \begin{cases} 0 & \gamma < \gamma_{\text{I.EGC}} \\ \frac{h^2}{R_{\text{I}}^2} \gamma_{\text{0.EGC}}^{\frac{1}{m+4}} \left(\gamma_{\text{I.EGC}}^{-\frac{1}{m+4}} - \gamma^{-\frac{1}{m+4}}\right) & \gamma_{\text{I.EGC}} \leq \gamma \leq \gamma_{\text{0.EGC}} \\ 1 & \gamma > \gamma_{\text{0.EGC}} \end{cases} \tag{59}$$

$$F_{\mathrm{O}}(\gamma)_{\mathrm{EGC}} = \frac{R_{\mathrm{I}}^2}{R_{\mathrm{II}}^2} F_{\mathrm{I}}(\gamma)_{\mathrm{EGC}} + \frac{R_{\mathrm{II}}^2 - R_{\mathrm{I}}^2}{R_{\mathrm{II}}^2} F_{\mathrm{II}}(\gamma)_{\mathrm{EGC}}. \tag{67}$$

C. SINR FOR MRC SCHEME

For MRC scheme, a similar approach as for EGC is considered. However, MRC applies a specific weight to each of the photodiodes that compose the ADR to maximize the SINR.

1) SCENARIO I ($0 \le R \le R_{\mathrm{I}}$)

It is worth recalling that in this case the main source of interference comes from the NLoS component. Therefore, the channel between optical AP l and photodiode i is equal to (54). Then, the resulting SINR in scenario I is given by

$$\gamma(r)_{\mathrm{MRC}} = \frac{\left(P_{\mathrm{t}} \sum_{i=1}^{N_{\mathrm{PD}}} w_i H_{l,i}(r, \Psi_{\mathrm{ADR}})\right)^2}{\sum_{i=1}^{N_{\mathrm{PD}}} w_i^2 \mathcal{I}_i^{\mathrm{NLoS}}(\Psi_{\mathrm{ADR}}) + \sum_{i=1}^{N_{\mathrm{PD}}} w_i^2 \sigma_n^2} \approx \frac{\left(P_{\mathrm{t}} \sum_{i=1}^{N_{\mathrm{PD}}} w_i H_{l,i}(r, \Psi_{\mathrm{ADR}})\right)^2}{\sum_{i=1}^{N_{\mathrm{PD}}} w_i^2 \mathcal{I}_i^{\mathrm{NLoS}}(\Psi_{\mathrm{ADR}})} \tag{68}$$

where

$$w_i = \frac{\left(P_{\mathrm{t}} H_i(\tilde{r}_{l,I}, \Psi_{\mathrm{ADR}})\right)^2}{\mathcal{I}_i^{\mathrm{NLoS}}(\Psi_{\mathrm{ADR}}) + \sigma_n^2}. \tag{69}$$

Following the same methodology as the derivation for EGC, the PDF and CDF for MRC scheme are the same as in (56) and (59), respectively, by simply substituting $\gamma(r)_{\mathrm{EGC}}$ for $\gamma(r)_{\mathrm{MRC}}$ and considering $\gamma_{0.\mathrm{MRC}}$ and $\gamma_{\mathrm{I.MRC}}$ as the SINR for MRC at $r = 0$ and $r = R_I$, respectively.

2) SCENARIO II ($R_{\mathrm{I}} \le R \le R_{\mathrm{II}}$)

For scenario II, the contribution of the LoS channel follows the same geometrical analysis as derived for EGC. Taking into consideration the impact of the weights of MRC, the resulting SINR in scenario II can be written as

$$\gamma(r)_{\mathrm{MRC}} \approx \frac{\left(\sum_{i=1}^{N_{\mathrm{PD}}} w_i H_{l,i}(r, \Psi_{\mathrm{ADR}})\right)^2}{\left(\sum_{i=1}^{N_{\mathrm{PD}}} w_i H_{l',i}(\tilde{r}_{l',II}, \Psi_{\mathrm{ADR}})\right)^2} = \frac{\left(\sum_{i=1}^{N_{\mathrm{PD}}} w_i Q_{l,i}\right)^2 (\tilde{r}_{l',II}^2 + h^2)^{4+m}}{\left(\sum_{i=1}^{N_{\mathrm{PD}}} w_i Q_{l',i}\right)^2 (r^2 + h^2)^{4+m}}, \tag{70}$$

where the coefficients $Q_{l,i}$ and $Q_{l',i}$ are as detailed in (61) for the EGC scheme and the weights of the MRC scheme are given by

$$w_i = \frac{(P_{\mathrm{t}} H_{l,i}(\tilde{r}_{l',I}, \Psi_{\mathrm{ADR}}))^2}{(P_{\mathrm{t}} H_{l',i}(\tilde{r}_{l',II}, \Psi_{\mathrm{ADR}}))^2 + \sigma_n^2}. \tag{71}$$

Similarly to previous schemes, applying the change of variable method and after some mathematical rearrangement, the PDF of SINR is given in (72), as shown at the bottom of the next page, where $\gamma'_{\mathrm{I.MRC}}$ and $\gamma_{\mathrm{II.MRC}}$ are the maximum and minimum values of the SINR in the region, which occurs at $r = R_{\mathrm{I}}$ and $r = R_{\mathrm{II}}$, respectively, i.e.,

$$\gamma'_{\mathrm{I.MRC}} = \frac{\left(\sum_{i=1}^{N_{\mathrm{PD}}} w_i Q_{l,i}\right)^2 \left(\tilde{r}_{l',II}^2 + h^2\right)^{4+m}}{\left(\sum_{i=1}^{N_{\mathrm{PD}}} w_i Q_{l',i}\right)^2 \left(R_{\mathrm{I}}^2 + h^2\right)^{4+m}}, \tag{73}$$

$$f_{\mathrm{II}}(\gamma)_{\mathrm{EGC}} = \begin{cases} \dfrac{1}{(m+4)(R_{\mathrm{II}}^2 - R_{\mathrm{I}}^2)} \left(\dfrac{\left(\sum_{i=1}^{N_{\mathrm{PD}}} Q_{l,i}\right)^2 \left(\tilde{r}_{l',II}^2 + h^2\right)^{4+m}}{\left(\sum_{i=1}^{N_{\mathrm{PD}}} Q_{l',i}\right)^2} \right)^{\frac{1}{m+4}} \gamma^{\frac{-(m+5)}{m+4}} & \gamma_{\mathrm{II.EGC}} \le \gamma \le \gamma'_{\mathrm{I.EGC}} \\ 0 & \text{otherwise} \end{cases} \tag{64}$$

$$F_{\mathrm{II}}(\gamma)_{\mathrm{EGC}} = \begin{cases} 0 & \gamma < \gamma_{\mathrm{II,EGC}} \\ \dfrac{1}{(R_{\mathrm{II}}^2 - R_{\mathrm{I}}^2)} \left(\dfrac{\left(\sum_{i=1}^{N_{\mathrm{PD}}} Q_{l,i}\right)^2 \left(\tilde{r}_{l',II}^2 + h^2\right)^{4+m}}{\left(\sum_{i=1}^{N_{\mathrm{PD}}} Q_{l',i}\right)^2} \right)^{\frac{1}{m+4}} \left(\gamma_{\mathrm{II.EGC}}^{-\frac{1}{m+4}} - \gamma^{-\frac{1}{m+4}}\right) & \gamma_{\mathrm{II.EGC}} \le \gamma \le \gamma'_{\mathrm{I.EGC}} \\ 1 & \gamma > \gamma'_{\mathrm{I.EGC}} \end{cases} \tag{65}$$

$$\gamma_{\text{II.MRC}} = \frac{\left(\sum_{i=1}^{N_{\text{PD}}} w_i Q_{l,i}\right)^2 \left(\tilde{r}_{l',II}^2 + h^2\right)^{4+m}}{\left(\sum_{i=1}^{N_{\text{PD}}} w_i Q_{l',i}\right)^2 (R_{\text{II}}^2 + h^2)^{4+m}}. \quad (74)$$

Then, by integrating the PDF, the CDF of SINR in scenario II is given in (75), as shown at the bottom of the next page.

3) OVERALL THEORETICAL SINR ($0 \leq R \leq R_{\text{II}}$)

Finally, the overall theoretical PDF and CDF of SINR in MRC scheme is given by

$$f_{\text{O}}(\gamma)_{\text{MRC}} = \begin{cases} \frac{R_{\text{II}}^2 - R_{\text{I}}^2}{R_{\text{II}}^2} f_{\text{II}}(\gamma)_{\text{MRC}} & \gamma_{\text{II.MRC}} \leq \gamma \leq \gamma'_{\text{I.MRC}} \\ \frac{R_{\text{I}}^2}{R_{\text{II}}^2} f_{\text{I}}(\gamma)_{\text{MRC}} & \gamma_{\text{I.MRC}} \leq \gamma \leq \gamma_{0.\text{MRC}} \\ 0 & \text{otherwise,} \end{cases} \quad (76)$$

$$F_{\text{O}}(\gamma)_{\text{MRC}} = \frac{R_{\text{I}}^2}{R_{\text{II}}^2} F_{\text{I}}(\gamma)_{\text{MRC}} + \frac{R_{\text{II}}^2 - R_{\text{I}}^2}{R_{\text{II}}^2} F_{\text{II}}(\gamma)_{\text{MRC}}. \quad (77)$$

It is worth remarking that the performance of the SINR for MRC in scenario I is expected to be similar as for EGC. This is because the weights of MRC depend on the NLoS interference, which remains the same for all photodiodes in the ADR. However, in scenario II, the weight of each photodiodes aims at maximizing the resulting SINR. As a result, it is expected that MRC outperforms EGC considerably in scenario II.

VI. SIMULATION RESULTS

Monte Carlo simulations are performed to discuss the accuracy of the theoretical derivation obtained in previous sections. For the sake of simplicity and facilitating the analysis, a scenario comprising two attocells is assumed. For single-PD architecture, the FoV is set to 33°. Two ADR configurations are analyzed comprising 4 and 12 photodiodes with a FoV equal to 28° and 23°, respectively. The resulting noise is calculated for a modulation bandwidth of 20 MHz assuming a noise spectral efficiency equal to 10^{-21} A/Hz [19]. Notice that the modulation bandwidth may comprise values from hundreds of KHz for mass-market commercial LEDs [31] to hundreds of MHz for some specific communications-oriented micro LEDs [32], [33]. All other simulation parameters are listed in Table. 1

TABLE 1. Simulation parameters.

Optical cell radius, R_{cell}	1.5 m
Height of optical APs , h	4 m
Detection Area of the photodiode, A	5 mm^2
Optical transmitter semi-angle, $\varphi_{1/2}$	60°
Gain of Optical filter, T_s	1
Reflective Index, n	1.5
Noise Power spectral density, N_0	1×10^{-21} A^2/Hz
Responsivity, τ	1 A/W
Transmitted optical power, P_{t}	1 W

First, the achievable user rate calculated as $\log_2(1+\text{SINR})$ for both single-PD and ADR assuming SBC is depicted in Fig. 12 with the aim of validating the approach based on dividing the coverage footprint into scenario I and scenario II. Specifically, a simulation is carried out assuming two optical APs located at $r = 0$ and $r = 2.6$ m. Moreover, the condition (35) or any other approximation in Section V is not considered. As expected, the user rate takes a maximum value at $r = 0$ and $r = 2.6$ m, which is denoted by $R_{\max}$. The region of scenario I comprises a range in which the rate $R_{\max}$ decreases to $\frac{R_{\max}}{\sqrt{2}}$ approximately. Then, it can be seen that the user rate abruptly decreases to values below 4 bits/sec/Hz because of the influence of the intercell interference. Therefore, we can conclude that the proposed approach based on dividing the coverage footprint of the optical AP into scenario I and II is appropriate.

With the aim of analyzing the performance enhancement introduced by the use of ADRs, the CDF of the SINR for both architectures single-PD and ADR assuming the SBC scheme are depicted in Fig. 13. It can be seen that the simulation results match with the theoretical derivations assuming some slight variations. Notice that there exists a gap about 5 dB between the single-PD and SBC, while in scenario II, the gap is around 3.5 dB. This difference can be attributed to the ability of SBC to select the photodiode that provides the highest channel gain with minimal interference from interference. It's worth noting that the numerical results for a single-PD and SBC in scenario II match with the theoretical results, although there is a very slight variation in the theoretical SINR for SBC in scenario II.

The CDFs of SINR for single-PD and ADR architectures assuming SBC, EGC, and MRC schemes are depicted in Fig. 14. The difference between the values obtained through

$$f_{\text{II}}(\gamma)_{\text{MRC}} = \begin{cases} \frac{1}{(m+4)(R_{\text{II}}^2 - R_{\text{I}}^2)} \left(\frac{\left(\sum_{i=1}^{N_{\text{PD}}} w_i Q_{l,i}\right)^2 \left(\tilde{r}_{l',II}^2 + h^2\right)^{4+m}}{\left(\sum_{i=1}^{N_{\text{PD}}} w_i Q_{l',i}\right)^2} \right)^{\frac{1}{m+4}} \gamma^{\frac{-(m+5)}{m+4}} & \gamma_{\text{II.MRC}} \leq \gamma \leq \gamma'_{\text{I.MRC}} \\ 0 & \text{otherwise} \end{cases} \quad (72)$$

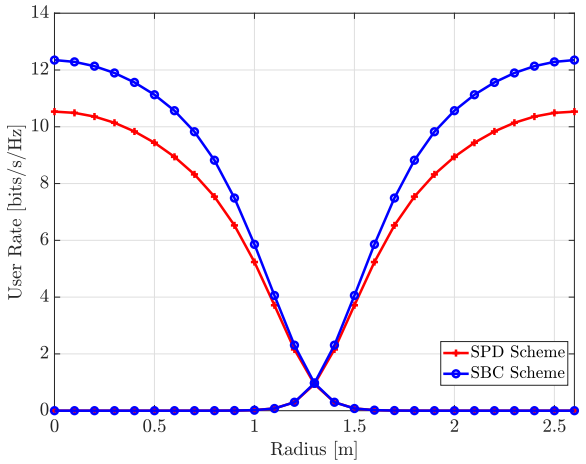

FIGURE 12. The overall user's rate for single PD and SBC schemes with respects to radius r, optical APs located at $r = 0$ and $r = 2.6$.

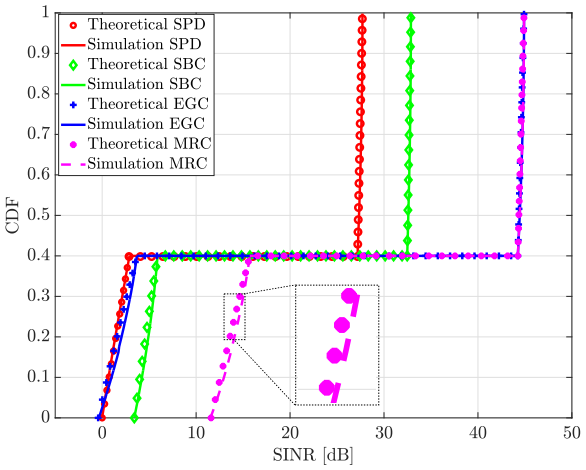

FIGURE 14. The overall CDF performance of SINR in SBC, EGC, and MRC schemes. Pyramid ADR used with four faces.

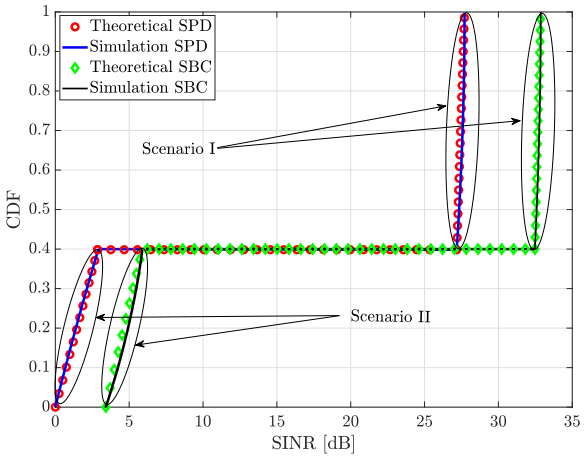

FIGURE 13. The overall CDF of SINR includes scenario I and II for single-PD and SBC, pyramid ADR with four faces.

simulations and the derived closed-form expressions is highlighted for MRC. Notice that the approximation errors generated by the considered assumptions are below 1 dB, i.e., they barely affect to the accuracy of the obtained results. Interestingly, both MRC and EGC achieve a similar performance in scenario I since the interference is mainly given by the NLoS component, which results similar in the whole set of photodiodes that compose the ADR. On the other hand, in scenario II, MRC achieves better results than all other schemes since the LoS contributions of the interference are managed through the weights (see (71)) in order to maximize the SINR. It can be also seen that single-PD and EGC obtain a similar performance in scenario II. Notice that for EGC, the ADR can be interpreted as a single photodiode that receives contributions from a very wide FoV. The SBC achieves indeed greater performance than EGC in scenario II because of the interference suppression given by selecting a unique photodiode from the set that compose the ADR.

In Fig. 15, the CDFs for ADRs composed of a larger number of photodiodes, specifically 12 photodiodes instead of 4, are depicted. As occurs for ADRs with 4 photodiodes (see Fig. 14), it can be seen that the closed-form expressions obtains values close to the simulation results. First, notice that the achieved SINR improves in comparison with the obtained for ADRs composed of 4 photodiodes (see Fig. 14). Moreover, in scenario II, the MRC outperforms all other schemes, which is more noticeable in scenario II. For MRC, the achievable SINR improves about 10 dB in comparison with the obtained for ADRs composed of four photodiodes. Moreover, it can be seen that there exists a gap of 20 dB and 18 dB between the SINR obtained by MRC and, EGC and SBC, respectively. It is worth noticing that a similar performance is achieved for EGC in scenario II as number of photodiodes that compose the ADRs increases because

$$F_{\text{II}}(\gamma)_{\text{MRC}} = \begin{cases} 0 & \gamma < \gamma_{\text{II,MRC}} \\ \dfrac{1}{(R_{\text{II}}^2 - R_{\text{I}}^2)} \left(\dfrac{\left(\sum_{i=1}^{N_{\text{PD}}} w_i Q_{l,i} \right)^2 \left(\tilde{r}_{l',II}^2 + h^2 \right)^{4+m}}{\left(\sum_{i=1}^{N_{\text{PD}}} w_i Q_{l',i} \right)^2} \right)^{\frac{1}{m+4}} \left(\gamma_{\text{II.MRC}}^{-\frac{1}{m+4}} - \gamma^{-\frac{1}{m+4}} \right) & \gamma_{\text{II.MRC}} \leq \gamma \leq \gamma'_{\text{I.MRC}} \\ 1 & \gamma > \gamma'_{\text{I.MRC}} \end{cases} \tag{75}$$

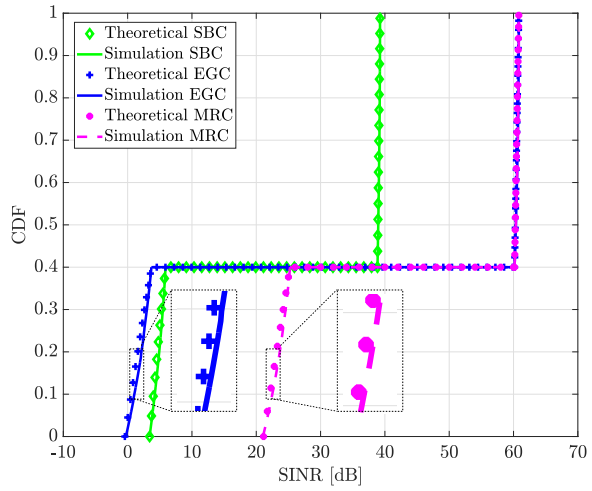

FIGURE 15. The overall CDF performance of SINR in SBC, EGC, and MRC schemes. Pyramid ADR used with 12 faces.

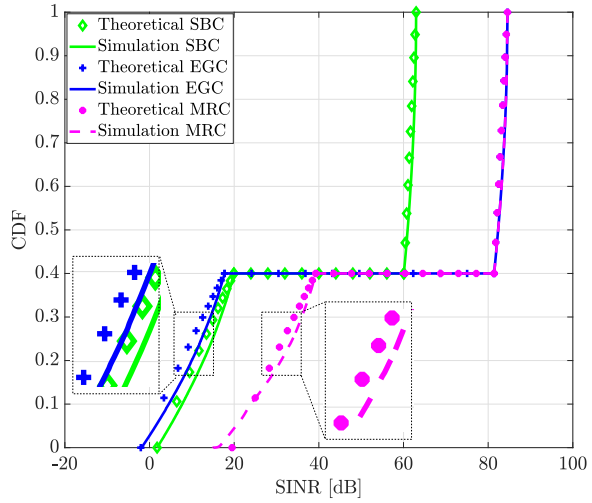

FIGURE 16. The overall CDF performance of SINR in SBC, EGC, and MRC schemes using narrow semi-angle $\varphi_{1/2} = 15^{o}$. Pyramid ADR used with 12 faces.

it simply generates a wider area of reception, which leads to increasing the intercell interference. For SBC, the SINR enhancement is clear in scenario I, but it slightly improves the SINR in scenario II.

In Fig. 16, the distribution of the SINR for narrow transmission semi-angles, specifically $\varphi_{1/2} = 15°$, is analyzed. That is, the light intensity is more concentrated in the center of the coverage footprint while reducing the region subject to high levels of intercell interference. In this case, it can be seen that greater approximation errors below 3 dB due the considered assumptions appear in comparison with the previous simulations for wider semi-angles. It can be seen that the SINR increases in both scenario I and II. For instance, the maximum SINR achieved in scenario II for this case is equal to 40 dB, in contrast to the 26 dB obtained in Fig. 15. Besides, it is worth noting that the slope of the SINR increases

TABLE 2. Average SINR [dB] for scenarios I and II.

Radiation semi-angle	Number of photodiodes	Scheme	Scenario I	Scenario II
$\varphi_{1/2} = 60°$	$N_{\mathrm{PD}} = 1$	SPD	27.5	1.83
	$N_{\mathrm{PD}} = 4$	SBC	32.7	5.14
		EGC	44.6	2.36
		MRC	44.74	14.5
	$N_{\mathrm{PD}} = 12$	SBC	38.8	5.07
		EGC	60.17	1.95
		MRC	60.73	23.95
$\varphi_{1/2} = 15°$	$N_{\mathrm{PD}} = 12$	SBC	61.65	11.67
		EGC	83.12	9.13
		MRC	83.81	30.71

for all the schemes due to the narrow beams generated by each optical AP.

A. INSIGHTS FROM THE OBTAINED RESULTS

The results obtained by the derived equations and through Monte Carlo simulations validate the approach based on dividing the coverage footprint into scenarios I and II. The average SINR obtained in each of these scenarios is summarized in Table 2 with the aim of providing insights as well as issues to be solved in future works.

Although high SINR values can be obtained in the inner of the coverage footprint (scenario I), which improve considerably using EGC or MRC, the SINR is still penalized at cell edge because of intercell interference. For instance, assuming EGC or MRC, a SINR enhancement about 17.1 dB and 32.67 dB occurs in scenario I for $N_{\mathrm{PD}} = 4$ and $N_{\mathrm{PD}} = 12$ photodiodes, respectively. On the other hand, SBC or EGC are considerably penalized in scenario II achieving low SINR, while MRC obtains a SINR increase of 12.7 dB and 22.1 dB for $N_{\mathrm{PD}} = 4$ and $N_{\mathrm{PD}} = 12$ photodiodes, respectively. Therefore, recalling that for non-overlapping FoV ADRs the intended signal is mainly received by a single photodiode, the signal and interference diversity provided by the proposed overlapping FoV ADRs allows us to achieve satisfactory SINR values for MRC.

Focusing on scenario II, for the SBC scheme, the improvement of the average SINR in comparison with SPD is about 5 dB for both $N_{\mathrm{PD}} = 4$ and $N_{\mathrm{PD}} = 12$ photodiodes. That is, the users are still subject to intercell interference. Interestingly, EGC is even more penalized than SBC since the receiver is subject to both intended signal and interference from a wide FoV obtained by selecting all the photodiodes of the ADR. In this sense, notice that MRC obtains greater SINR than both SBC and EGC. Specifically, an average SINR equal to 14.5 dB and 23.95 dB is obtained in scenario II for $N_{\mathrm{PD}} = 4$ and $N_{\mathrm{PD}} = 12$ photodiodes, respectively. That is, managing the intercell interference still requires some complex signal processing based on CSI as occurs for MRC. Although the SINR obtained by MRC in scenario II outperforms EGC or SBC, it is worth remarking that there still exists a considerable gap between the SINR in scenarios I and II.

The discussion of the results described above motivates the use of a central unit for managing the transmission strategy depending of the position of the optical APs and the users. For instance, users located within the cell center (scenario I) obtain high SINR, which increase using overlapping FoV ADRs considering simple signal processing such as SBC or EGC. However, with the aim of avoiding complex signal processing based on calculating weights, which requires additional signalling for providing CSI, interference management can be potentially applied. Considering time division multiple access (TDMA) for the sake of simplicity, the intercell interference in scenario II can be avoided assigning an orthogonal time slot to each user at the cost of penalizing the achievable degrees of freedom, i.e., the user rate would be multiplied by the percentage of time allocated to that user. On the other hand, it is worth noticing that this topological approach requires obtaining knowledge about the position of the users and determining if they are limited by intercell interference or not. Furthermore, more complex interference management based on precoding techniques such as ZF can be applied, increasing the amount of signaling to provide CSI at the transmitter side.

It can be also seen that reducing the radiation semi-angle generates small and more confined coverage footprints. Therefore, high SINR can be achieved within a region while reducing the intercell interference out of that region, which motivates a user-centric approach [8]. Notice that user-centric schemes require a central unit and more accurate knowledge of the position of the users than the topological interference management based on orthogonal resource allocation suggested above. Therefore, we can conclude that obtaining knowledge about the position of the users may improve considerably the SINR without the need for CSI, which motivate the development of simultaneous transmission and positioning schemes for VLC.

B. REAL-WORLD TESTING: DISCUSSION AND RESULTS

This subsection is devoted to provide a methodology to implement a real-world testing of the statistical characteristics of the SINR for overlapping FoV ADRs. After that, some experimental results are presented and discussed and further research lines are considered.

First, notice that a statistical analysis requires a large number of samples to obtain accurate results. To do that, we propose the implementation of an actuation rod in which two servomotors modify the longitudinal dimension and the azimuthal angle of the photodetector as it is shown in Fig. 17. That is, the longitudinal variable, modified by servomotor A, moves the receiver from the intended to the interfering optical APs while servomotor B allows us to measure the received power for different azimuthal angles subject to a fixed elevation angle, i.e., similarly to a pyramidal arrangement. The electronic architecture of the optical AP and receiver are based on the schemes proposed in [34]. Thus, a known pattern is transmitted as a reference (pilot) signal to

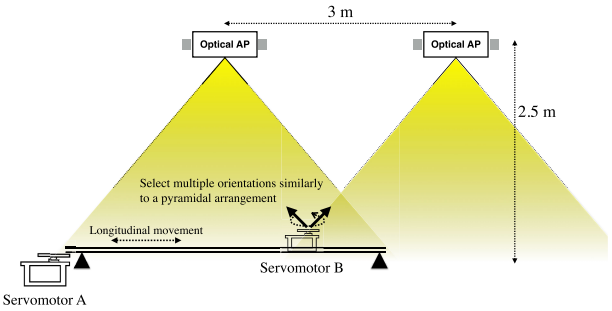

FIGURE 17. Measurement set-up based on an actuation rod and two servomotors. Servomotor A varies the longitudinal dimension along the rod and servomotor B modifies the azimuthal angle among a set of values subject to a fixed elevation angle similarly to a pyramidal arrangement.

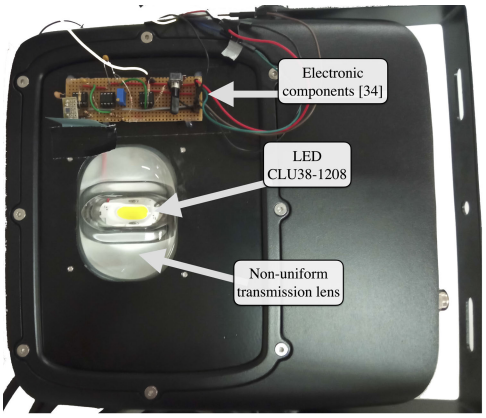

FIGURE 18. Optical AP employed in the testbed.

estimate the channel at the receiver and stored it in a dataset afterwards. The optical APs are based on the LED CLU038-1208 of Citizen, whose electrical dynamic behaviour, i.e., the modulation bandwidth, is fully characterized in [31]. The receiver corresponds to the photodetector ThorLabs PDA100A2 [35].

After a brief measurement campaign following the scheme described in Fig. 17 in a laboratory of Universidad Carlos III de Madrid, the obtained dataset generates a CDF as depicted in Fig. 19. Specifically, servomotor B considers steps comprising 45° in the azimuthal range (360°) and a fixed elevation angle equal to 30°. The signals from the intended and interfering optical APs are received independently, and the resulting SINR is calculated afterwards assuming a SBC scheme. First, it can be seen that the approach based on dividing the coverage footprint into scenarios I and II is satisfied in a real-world testing. Interestingly, scenario II occupies a larger region of SINR than scenario I since the optical AP is equipped with a non-uniform lens than concentrate the signal in the longitudinal axis as can be seen in Fig. 18.

We can conclude that the obtained preliminary results validate the approach considered in this work. However, further investigations considering multiple APs, i.e., different

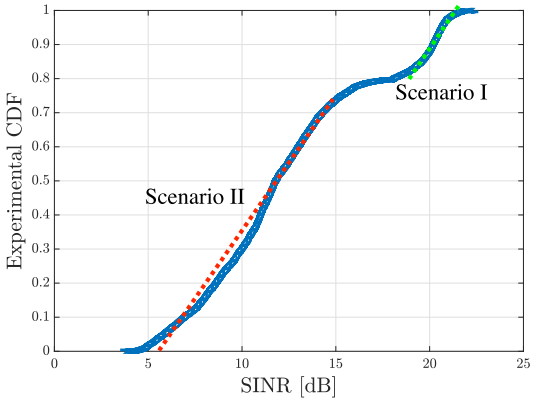

FIGURE 19. Experimental CDF obtained in the considered set-up.

LEDs that may be equipped with a set of concentrator lenses, set-up configurations or propagation environments are required for a complete characterization of the SINR in a real-world testing. It is worth noticing that this characterization would generate a very large dataset of realistic measurements, which could be extended considering additional parameters such as level of illumination, presence of blocking, or the environment characteristics, e.g., office, residential, industrial, etc., that can be useful to determine the impact of realistic datasets in comparison with synthetic datasets for feeding artificial intelligence algorithms.

VII. CONCLUSION

In this work, we analyze the statistical distribution of the SINR assuming ADRs composed of photodiodes whose FoV overlap among them in VLC networks. The derivation of the statistical distributions subject to this ADR architecture is obtained considering assumptions that allow us to approximate the sum of the cosine of the incidence angles of the proposed ADR. The proposed approach is also validated through an experimental testbed. Specifically, the statistical distribution of the SINR is derived for the SBC, EGC, and MRC schemes. Assuming a wide FoV of the photodiodes that compose the ADR, an error below 1 dB between Monte Carlo simulations and the derived closed-form expressions is obtained. This error is lower than 3 dB for photodiodes with a narrow FoV, e.g., 15°. Our findings indicate that MRC outperforms all other schemes, particularly in regions with high levels of intercell interference. This SINR improvement is greater than 10 dB in the considered scenarios and may increase assuming a greater number of photodiodes per ADR or reducing the semi-angle of the optical APs.

REFERENCES

[1] N. Chi, Y. Zhou, Y. Wei, and F. Hu, "Visible light communication in 6G: Advances, challenges, and prospects," *IEEE Veh. Technol. Mag.*, vol. 15, no. 4, pp. 93–102, Dec. 2020.

[2] D. H. Mai, H. D. Le, T. V. Pham, and A. T. Pham, "Design and performance evaluation of large-scale VLC-based indoor positioning systems under impact of receiver orientation," *IEEE Access*, vol. 8, pp. 61891–61904, 2020.

[3] M. M. Céspedes, B. G. Guzmán, V. P. Gil Jiménez, and A. G. Armada, "Aligning the light for vehicular visible light communications: High data rate and low-latency vehicular visible light communications implementing blind interference alignment," *IEEE Veh. Technol. Mag.*, vol. 18, no. 1, pp. 59–69, Mar. 2023.

[4] L. E. M. Matheus, A. B. Vieira, L. F. M. Vieira, M. A. M. Vieira, and O. Gnawali, "Visible light communication: Concepts, applications and challenges," *IEEE Commun. Surveys Tuts.*, vol. 21, no. 4, pp. 3204–3237, 4th Quart., 2019.

[5] C. Chen, N. Serafimovski, and H. Haas, "Fractional frequency reuse in optical wireless cellular networks," in *Proc. IEEE 24th Annu. Int. Symp. Pers., Indoor, Mobile Radio Commun. (PIMRC)*, Sep. 2013, pp. 3594–3598.

[6] T. V. Pham, H. Le-Minh, and A. T. Pham, "Multi-user visible light communication broadcast channels with zero-forcing precoding," *IEEE Trans. Commun.*, vol. 65, no. 6, pp. 2509–2521, Jun. 2017.

[7] M. M. Céspedes, B. G. Guzmán, and V. P. G. Jiménez, "Lights and shadows: A comprehensive survey on cooperative and precoding schemes to overcome LOS blockage and interference in indoor VLC," *Sensors*, vol. 21, no. 3, p. 861, Jan. 2021.

[8] A. A. Qidan, M. Morales-Céspedes, A. G. Armada, and J. M. H. Elmirghani, "Resource allocation in user-centric optical wireless cellular networks based on blind interference alignment," *J. Lightw. Technol.*, vol. 39, no. 21, pp. 6695–6711, Nov. 2021.

[9] C. He, S. Cincotta, M. M. A. Mohammed, and J. Armstrong, "Angular diversity aperture (ADA) receivers for indoor multiple-input multiple-output (MIMO) visible light communications (VLC)," *IEEE Access*, vol. 7, pp. 145282–145301, 2019.

[10] A. G. Al-Sakkaf and M. Morales-Céspedes, "On the coverage footprint for high-capacity VLC through angle diversity receivers," in *Proc. IEEE Globecom Workshops (GC Wkshps)*, Dec. 2023, pp. 685–690.

[11] A. Nuwanpriya, S.-W. Ho, and C. S. Chen, "Indoor MIMO visible light communications: Novel angle diversity receivers for mobile users," *IEEE J. Sel. Areas Commun.*, vol. 33, no. 9, pp. 1780–1792, Sep. 2015.

[12] E. Sarbazi, H. Kazemi, M. Crisp, T. El-Gorashi, J. Elmirghani, R. Penty, I. White, M. Safari, and H. Haas, "Design and optimisation of high-speed receivers for 6G optical wireless networks," *IEEE Trans. Commun.*, vol. 72, no. 2, pp. 971–990, Feb. 2024.

[13] D. K. Tettey, M. Elamassie, and M. Uysal, "Experimental investigation of angle diversity receiver for vehicular VLC," in *Proc. 29th Annu. Int. Conf. Mobile Comput. Netw.* New York, NY, USA: Association for Computing Machinery, Oct. 2023, pp. 1–3.

[14] P. Palacios Játiva, M. Román Cañizares, C. A. Azurdia-Meza, D. Zabala-Blanco, A. Dehghan Firoozabadi, F. Seguel, S. Montejo-Sánchez, and I. Soto, "Interference mitigation for visible light communications in underground mines using angle diversity receivers," *Sensors*, vol. 20, no. 2, p. 367, Jan. 2020.

[15] P. P. Játiva, C. A. Azurdia-Meza, D. Zabala-Blanco, I. Soto, M. Ijaz, D. F. Carrera, and S. Ekpo, "On the performance of angular diversity receivers in underground mining VLC systems," in *Proc. 13th Int. Symp. Commun. Syst., Netw. Digit. Signal Process. (CSNDSP)*, Jul. 2022, pp. 795–800.

[16] M. Morales-Céspedes, A. A. Quidan, and A. G. Armada, "Experimental evaluation of the reconfigurable photodetector for blind interference alignment in visible light communications," in *Proc. 27th Eur. Signal Process. Conf. (EUSIPCO)*, Sep. 2019, pp. 1–5.

[17] P. Palacios Játiva, I. Sánchez, I. Soto, C. A. Azurdia-Meza, D. Zabala-Blanco, M. Ijaz, A. Dehghan Firoozabadi, and D. Plets, "A novel and adaptive angle diversity-based receiver for 6G underground mining VLC systems," *Entropy*, vol. 24, no. 11, p. 1507, Oct. 2022.

[18] A. Gupta and P. Garg, "Statistics of SNR for an indoor VLC system and its applications in system performance," *IEEE Commun. Lett.*, vol. 22, no. 9, pp. 1898–1901, Sep. 2018.

[19] Z. Chen, D. A. Basnayaka, X. Wu, and H. Haas, "Interference mitigation for indoor optical attocell networks using an angle diversity receiver," *J. Lightw. Technol.*, vol. 36, no. 18, pp. 3866–3881, Sep. 2018.

[20] M. Dehghani Soltani, A. A. Purwita, I. Tavakkolnia, H. Haas, and M. Safari, "Impact of device orientation on error performance of LiFi systems," *IEEE Access*, vol. 7, pp. 41690–41701, 2019.

[21] M. Morales-Céspedes, H. Haas, and A. G. Armada, "Optimization of the receiving orientation angle for zero-forcing precoding in VLC," *IEEE Commun. Lett.*, vol. 25, no. 3, pp. 921–925, Mar. 2021.

[22] M. Hosney, H. A. I. Selmy, A. Srivastava, and K. M. F. Elsayed, "Interference mitigation using angular diversity receiver with efficient channel estimation in MIMO VLC," *IEEE Access*, vol. 8, pp. 54060–54073, 2020.
[23] S. Saeedi, A. C. M. Fong, S. P. Mohanty, A. K. Gupta, and S. Carr, "Consumer artificial intelligence mishaps and mitigation strategies," *IEEE Consum. Electron. Mag.*, vol. 11, no. 3, pp. 13–24, May 2022.
[24] J. M. Kahn and J. R. Barry, "Wireless infrared communications," *Proc. IEEE*, vol. 85, no. 2, pp. 265–298, Feb. 1997.
[25] Z. Chen, D. Tsonev, and H. Haas, "Improving SINR in indoor cellular visible light communication networks," in *Proc. IEEE Int. Conf. Commun. (ICC)*, Jun. 2014, pp. 3383–3388.
[26] F. E. Alsaadi and J. M. H. Elmirghani, "Mobile MC-CDMA optical wireless system employing an adaptive multibeam transmitter and diversity receivers in a real indoor environment," in *Proc. IEEE Int. Conf. Commun.*, 2008, pp. 5196–5203.
[27] Z. Chen, N. Serafimovski, and H. Haas, "Angle diversity for an indoor cellular visible light communication system," in *Proc. IEEE 79th Veh. Technol. Conf. (VTC Spring)*, May 2014, pp. 1–5.
[28] C. Chen, S. Videv, D. Tsonev, and H. Haas, "Fractional frequency reuse in DCO-OFDM-based optical attocell networks," *J. Lightw. Technol.*, vol. 33, no. 19, pp. 3986–4000, Oct. 1, 2015.
[29] S.-H. Chang, H.-G. Park, S.-H. Kim, and J. P. Choi, "Study on coverage of full frequency reuse in FFR systems based on outage probability," *IEEE Trans. Commun.*, vol. 66, no. 11, pp. 5828–5843, Nov. 2018.
[30] Y. S. Eroglu, I. Güvenç, A. Sahin, Y. Yapici, N. Pala, and M. Yüksel, "Multi-element VLC networks: LED assignment, power control, and optimum combining," *IEEE J. Sel. Areas Commun.*, vol. 36, no. 1, pp. 121–135, Jan. 2018.
[31] J. S. B. Perlaza, J. C. T. Zafra, M. Morales-Cespedes, A. A. Qidan, B. Bentura, A. G. Armada, and J. M. S. Pena, "Measurement of the modulation bandwidth of high-power chip-on-board LEDs for VLC systems," in *Proc. 13th Int. Symp. Commun. Syst., Netw. Digit. Signal Process. (CSNDSP)*, Mar. 2022, pp. 38–42.
[32] H.-Y. Lan, I.-C. Tseng, H.-Y. Kao, Y.-H. Lin, G.-R. Lin, and C.-H. Wu, "752-MHz modulation bandwidth of high-speed blue micro light-emitting diodes," *IEEE J. Quantum Electron.*, vol. 54, no. 5, pp. 1–6, Oct. 2018.
[33] F. Xu, Z. Jin, T. Tao, P. Tian, G. Wang, X. Liu, T. Zhi, Q.-A. Yan, D. Pan, Z. Xie, K. Xu, B. Liu, and R. Zhang, "C-plane blue micro-LED with 1.53 GHz bandwidth for high-speed visible light communication," *IEEE Electron Device Lett.*, vol. 43, no. 6, pp. 910–913, Jun. 2022.
[34] M. M. Céspedes and A. G. Al-Sakkaf, "Visible light communications for IoT services based on high-power LEDs in Industry 4.0," in *Proc. IEEE Conf. Standards Commun. Netw. (CSCN)*, Nov. 2022, p. 89.
[35] Thorlabs, Datasheet. (2019). *PDA100A2—Si Fixed Gain Detector*. [Online]. Available: https://www.thorlabs.com/thorproduct.cfm?partnumber=PDA100A2

AHMED GAAFAR AHMED AL-SAKKAF received the B.Sc. and M.Sc. degrees in telecommunication engineering from Malaysia, in 2012 and 2015, respectively. He is currently pursuing the Ph.D. degree with the Department of Signal Theory and Communications, Universidad Carlos III de Madrid, under the EC-funded project MSCA ETN (TeamUp5G). His research interests include visible light communication, interference management, the IoT, and non-orthogonal multiple access (NOMA). In 2016, he was selected as the first Yemeni candidate for the Erasmus Mundus Program in smart systems integration, which was awarded by three universities in three different countries, such as Scotland, Norway, and Hungary.

MÁXIMO MORALES-CÉSPEDES (Member, IEEE) was born in Valdepeñas, Ciudad Real, Spain, in 1986. He received the B.Sc., M.Sc., and Ph.D. degrees in electrical engineering from Universidad Carlos III de Madrid, Spain, in 2010, 2012, and 2015, respectively, with a specialization in multimedia and communications. From 2015 to 2017, he was a Postdoctoral Fellow with the Institute of Information and Communication Technologies, Electronics and Applied Mathematics (ICTEAM), Université Catholique de Louvain. He is currently with the Department of Signal Theory and Communications, Universidad Carlos III de Madrid, Spain. His research interests include interference management, hardware implementations, MIMO techniques, and signal processing applied to wireless communications. He has been a TPC Member for numerous IEEE conferences, such as VTC, Globecom, ICC, and WCNC. In 2012, he was a Finalist of the IEEE Region 8 Student Paper Contest. He serves as an Editor for IEEE COMMUNICATION LETTERS.